Article

Cell Reports

PD-1 blockade therapy promotes infiltration of tumor-attacking exhausted T cell clonotypes

Graphical abstract

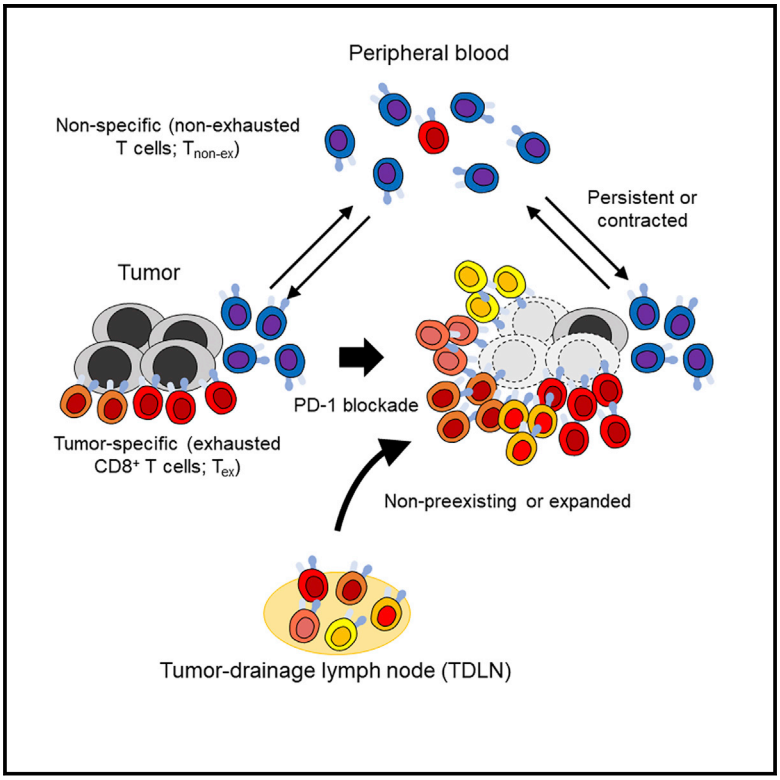

Authors

Joji Nagasaki, Takashi Inozume, Nicolas Sax, ..., Yutaka Suzuki, Hiroyoshi Nishikawa, Yosuke Togashi

Correspondence

ytogashi1584@gmail.com (Y.T.), hnishika@ncc.go.jp (H.N.)

In brief

Nagasaki et al. demonstrate that tumor-infiltrating skewed T cell clonotypes with an exhausted phenotype (T_{ex}) directly attack tumor cells. PD-1 blockade therapy can promote expansion of preexisting tumor-specific T_{ex} clonotypes, and infiltration of non-preexisting T_{ex} clonotypes, mainly from tumor-draining lymph nodes.

Highlights

- The tumor microenvironment has both skewed T_{ex} and T_{non-ex} clonotypes
- Among skewed clonotypes, T_{ex}, but not T_{non-ex}, directly attack tumor cells
- PD-1 blockade promotes T_{ex} clonotype infiltration
- TDLNs can be the origin of such T_{ex} clonotypes

Nagasaki et al., 2022, Cell Reports *38*, 110331
February 1, 2022
https://doi.org/10.1016/j.celrep.2022.110331

CellPress

Cell Reports

CellPress
OPEN ACCESS

Article

PD-1 blockade therapy promotes infiltration of tumor-attacking exhausted T cell clonotypes

Joji Nagasaki,[1,2,3] Takashi Inozume,[1,4,5] Nicolas Sax,[6] Ryo Ariyasu,[2] Masakazu Ishikawa,[6] Kazuo Yamashita,[6] Masahito Kawazu,[7] Toshihide Ueno,[7] Takuma Irie,[2] Etsuko Tanji,[1] Takao Morinaga,[1] Akiko Honobe,[5] Takehiro Ohnuma,[5] Mitsuru Yoshino,[8] Takekazu Iwata,[8] Katsushige Kawase,[1,9,10] Keita Sasaki,[9] Toyoyuki Hanazawa,[10] Vitaly Kochin,[11] Tatsuyoshi Kawamura,[5] Hiroyuki Matsue,[4] Masayuki Hino,[3] Hiroyuki Mano,[7] Yutaka Suzuki,[12] Hiroyoshi Nishikawa,[2,11,*] and Yosuke Togashi[1,2,13,14,*]

[1]Chiba Cancer Center, Research Institute, 666-2 Nitona-cho, Chuo-ku, Chiba 260-8717, Japan
[2]Division of Cancer Immunology, National Cancer Center, Research Institute, Exploratory Oncology Research and Clinical Trial Center (EPOC), 6-5-1 Kashiwanoha, Tokyo 104-0045, Kashiwa 277-8577, Japan
[3]Department of Hematology, Graduate School of Medicine, Osaka City University, Osaka 545-8585, Japan
[4]Department of Dermatology, Chiba University Graduate School of Medicine, Chiba 260-8670, Japan
[5]Department of Dermatology, University of Yamanashi, Chuo, Japan
[6]KOTAI Biotechnologies, Inc., Osaka 565-0871, Japan
[7]Division of Cellular Signaling, National Cancer Center, Research Institute, Tokyo 104-0045, Japan
[8]Department of Thoracic Surgery, Chiba Cancer Center, Chiba 260-8717, Japan
[9]Department of Head and Neck Surgery, Chiba Cancer Center, Chiba 260-8717, Japan
[10]Department of Otolaryngology, Head and Neck Surgery, Chiba University Graduate School of Medicine, Chiba 260-8670, Japan
[11]Department of Immunology, Nagoya University Graduate School of Medicine, Nagoya 466–8550, Japan
[12]Department of Computational Biology and Medical Sciences, Graduate School of Frontier Sciences, The University of Tokyo, Kashiwa 277-8568, Japan
[13]Department of Tumor Microenvironment, Okayama University Graduate School of Medicine, Dentistry and Pharmaceutical Sciences, Okayama 700-0932, Japan
[14]Lead contact
*Correspondence: ytogashi1584@gmail.com (Y.T.), hnishika@ncc.go.jp (H.N.)
https://doi.org/10.1016/j.celrep.2022.110331

SUMMARY

PD-1 blockade exerts clinical efficacy against various types of cancer by reinvigorating T cells that directly attack tumor cells (tumor-specific T cells) in the tumor microenvironment (TME), and tumor-infiltrating lymphocytes (TILs) also comprise nonspecific bystander T cells. Here, using single-cell sequencing, we show that TILs include skewed T cell clonotypes, which are characterized by exhaustion (T_{ex}) or nonexhaustion signatures ($T_{non\text{-}ex}$). Among skewed clonotypes, those in the T_{ex}, but not those in the $T_{non\text{-}ex}$, cluster respond to autologous tumor cell lines. After PD-1 blockade, non-preexisting tumor-specific clonotypes in the T_{ex} cluster appear in the TME. Tumor-draining lymph nodes (TDLNs) without metastasis harbor a considerable number of such clonotypes, whereas these clonotypes are rarely detected in peripheral blood. We propose that tumor-infiltrating skewed T cell clonotypes with an exhausted phenotype directly attack tumor cells and that PD-1 blockade can promote infiltration of such T_{ex} clonotypes, mainly from TDLNs.

INTRODUCTION

The gain of immune escape mechanism(s), including increases in the expression of various immunosuppressive molecules, such as PD-1/PD-1 ligands, is an important process during cancer development and progression (Schreiber et al., 2011; Topalian et al., 2015; Zou et al., 2016). Therefore, inhibition of such molecules with monoclonal antibodies (mAbs) has been tested in the clinic, and PD-1 blockade therapies have been shown to be effective against various types of cancer (Borghaei et al., 2015; Brahmer et al., 2015; Ferris et al., 2016; Hodi et al., 2010; Larkin et al., 2015; Topalian et al., 2015; Zou et al., 2016).

PD-1, which interacts with PD-1 ligands, is primarily expressed following the activation of T cells and suppresses T cell function, causing T cells to fall into a dysfunctional state called exhaustion (Blank et al., 2019; Wherry, 2011; Wherry and Kurachi, 2015). PD-1 blockade reinvigorates exhausted $CD8^+$ T cells (T_{ex}), leading to tumor regression (Topalian et al., 2015; Zou et al., 2016). While tumor-infiltrating $CD8^+$ T cells reportedly play a crucial role in PD-1 blockade-mediated antitumor immunity (Herbst et al., 2014; Topalian et al., 2015; Tumeh et al., 2014; Zou et al., 2016), tumor-infiltrating $CD8^+$ T cells do not always attack tumor cells, and they frequently contain nonspecific bystander T cells (Oliveira et al., 2021; Scheper et al., 2019; Simoni et al., 2018). T cells recognize cancer antigens presented on the major histocompatibility complex (MHC) through their T cell receptors (TCRs) (Coulie et al., 2014; Hulpke and Tampe, 2013). Thus, TCR analysis can be used to identify

tumor-specific T cells. Indeed, a previous study demonstrated that tumor-infiltrating PD-1^{+}CD8^{+} T cells possess clonal TCR repertoires that respond to tumor cells (Gros et al., 2014). Another study showed that T cells in tumor samples obtained from patients who respond to PD-1 blockade exhibit a highly skewed clonal TCR repertoire (Amaria et al., 2018; Bassez et al., 2021; Forde et al., 2018; Sade-Feldman et al., 2018; Tumeh et al., 2014; Yost et al., 2019). Therefore, skewed T cell clonotypes in the tumor microenvironment (TME) may represent tumor-specific T cells.

Recent progress in single-cell RNA sequencing (scRNA-seq) has impacted broad areas of cancer research and improved our understanding of the TME (Lim et al., 2020; Papalexi and Satija, 2018; Stuart and Satija, 2019). Moreover, it is now possible to integrate transcriptome and TCR sequencing at the single-cell level (scTCR-seq). Several recent studies using this technology have revealed that skewed T cell clonotypes bear high expression of well-known exhaustion signature genes, such as *PDCD1*, *TNFRSF9*, *ENTPD1*, and *ITGAE* (encoding PD-1, 4-1BB, CD39, and CD103, respectively) and that such T_{ex} clonotypes are expected to be tumor specific (Li et al., 2019; Sade-Feldman et al., 2018; Tirosh et al., 2016). Other studies provide evidence of the dynamic change in tumor-infiltrating T cell clonotypes after PD-1 blockade (Bassez et al., 2021; Yost et al., 2019). However, the actual tumor specificity—that is, which tumor antigens are recognized by tumor-infiltrating T cells—has not been fully examined (Oliveira et al., 2021). In addition, it remains unclear how PD-1 blockade influences this dynamic clonal change.

In this study, we used both scRNA-seq and scTCR-seq to analyze tumor-infiltrating T cells from melanoma patients treated with an anti-PD-1 mAb. Tumor-infiltrating T cells presented skewed T cell clonotypes, which were characterized by exhaustion or nonexhaustion signatures ($T_{non\text{-}ex}$). Among them, the skewed clonotypes in the T_{ex}, but not those in the $T_{non\text{-}ex}$, cluster responded to autologous tumor cell lines. Following PD-1 blockade, preexisting tumor-specific T_{ex} clonotypes expanded, and other clonotypes in the T_{ex} cluster also appeared in the TME of a superresponder. These non-preexisting clonotypes responded to not only posttreatment but also pretreatment autologous cancer cell lines. Thus, this appearance of clonotypes in the T_{ex} cluster was promoted by PD-1 blockade. While such T_{ex} clonotypes were rarely found in the peripheral blood, considerable numbers of these cells were detected in tumor-draining lymph nodes (TDLNs). FTY720, which locks lymphocytes in LNs, negated the efficacy of PD-1 blockade, significantly decreased T_{ex} infiltration, and abolished the increased T_{ex} infiltration after PD-1 blockade in mouse models. Hence, skewed clonotypes in the T_{ex} cluster are tumor specific, and PD-1 blockade promotes such T_{ex} clonal expansion and infiltration from TDLNs, resulting in PD-1 blockade-mediated antitumor immunity.

RESULTS

PD-1 blockade superresponders have a considerable population of skewed T_{ex} clonotypes in the TME

First, we used both droplet-based 5′ scRNA-seq and scTCR-seq to analyze four tumor-infiltrating T cell samples from three melanoma patients who received PD-1 blockade therapy. Patient characteristics are summarized in Table S1. MEL01 acquired resistance due to the loss of *B2M* after the initial response to PD-1 blockade, as previously reported (Inozume et al., 2019). In contrast, MEL02 and 03 achieved complete responses to PD-1 blockade therapy during more than 2 years (superresponders) (Table S1; Figure S1). Tumor-infiltrating lymphocytes (TILs) were obtained from MEL01 at the appearance of acquired resistance (Inozume et al., 2019) and from MEL03 before the initiation of PD-1 blockade therapy (Table S1; Figure S1). In MEL02, because only the inguinal lymph node (LN) metastasis did not radiologically respond, surgical resection was performed after the treatment (Table S1; Figure S1). Then, TILs from site-matched tumors were collected before PD-1 blockade therapy (MEL02-1) and after treatment (MEL02-2) (Figure S1). Severe inflammation with CD8^{+} T cell infiltration and reduced residual tumor cells upon PD-1 blockade were observed in the lesion (MEL02-2) with pathological analyses, indicating a favorable response in MEL02 (Figure S1).

We obtained paired TCR sequences in 34,033 out of 42,617 T cells (79.9%, Table S2). T cells were classified into eight clusters based on gene expression profiling, as previously reported (Figures 1A, 1B, and S2A; Table S3) (Yost et al., 2019). The regulatory T (T_{reg}) cell cluster accounted for more than 10% of all samples from tumor tissues, which is consistent with our previous studies (Kamada et al., 2019; Kumagai et al., 2020a, 2020b; Togashi et al., 2019). The three tumor samples from two responders contained a considerable population of the T_{ex} cluster, which was characterized by exhaustion-associated signature genes, such as *PDCD1*, *TNFRSF9*, *ENTPD1*, and *ITGAE* (Figures 1A, 1B, and S2B). We next focused on T cell clonotypes since skewed T cell clonotypes in the TME are expected to be tumor specific (Gros et al., 2014; Li et al., 2019; Tirosh et al., 2016; Tumeh et al., 2014). The sensitive tumor samples (MEL02-1, MEL02-2, and MEL03) had skewed clonotypes, especially in the T_{ex} cluster (Figures 1C and 1D). In contrast, T cells in the resistant sample (MEL01) had highly diverse clonotypes compared with those in the sensitive samples (Figures 1C and 1D). In addition to the T_{ex} cluster, $T_{non\text{-}ex}$ clusters also possessed considerably skewed clonotypes (Figure 1D). These findings suggest that skewed T_{ex} clonotypes in the TME may play an important role in PD-1 blockade-mediated antitumor immunity, although skewed T cell clonotypes are detected in both T_{ex} and $T_{non\text{-}ex}$ clusters.

Skewed clonotypes in the T_{ex} but not the $T_{non\text{-}ex}$ clusters from the TME are tumor specific

We previously obtained a tumor-specific T cell clone from MEL01 TILs (named clone #01) (Figure S3A; Table S4) (Inozume et al., 2019). Similarly, two T cell clones were developed from MEL02-1 TILs (named clones #02-4 and #02-5) (Figure S3A; Table S4), and the IFN-γ response and killing activity of each T cell clone were observed against an autologous tumor cell line (Figures 2A and 2B). Then, three clonotypes from these T cell clones were highlighted in the UMAP figure, showing that clones #02-4 and #02-5 in MEL02-1 were highly skewed in the T_{ex} cluster (49/66 and 175/194, respectively) (Figure 2C); thus suggesting that, among the skewed clonotypes, those in the T_{ex} cluster are tumor

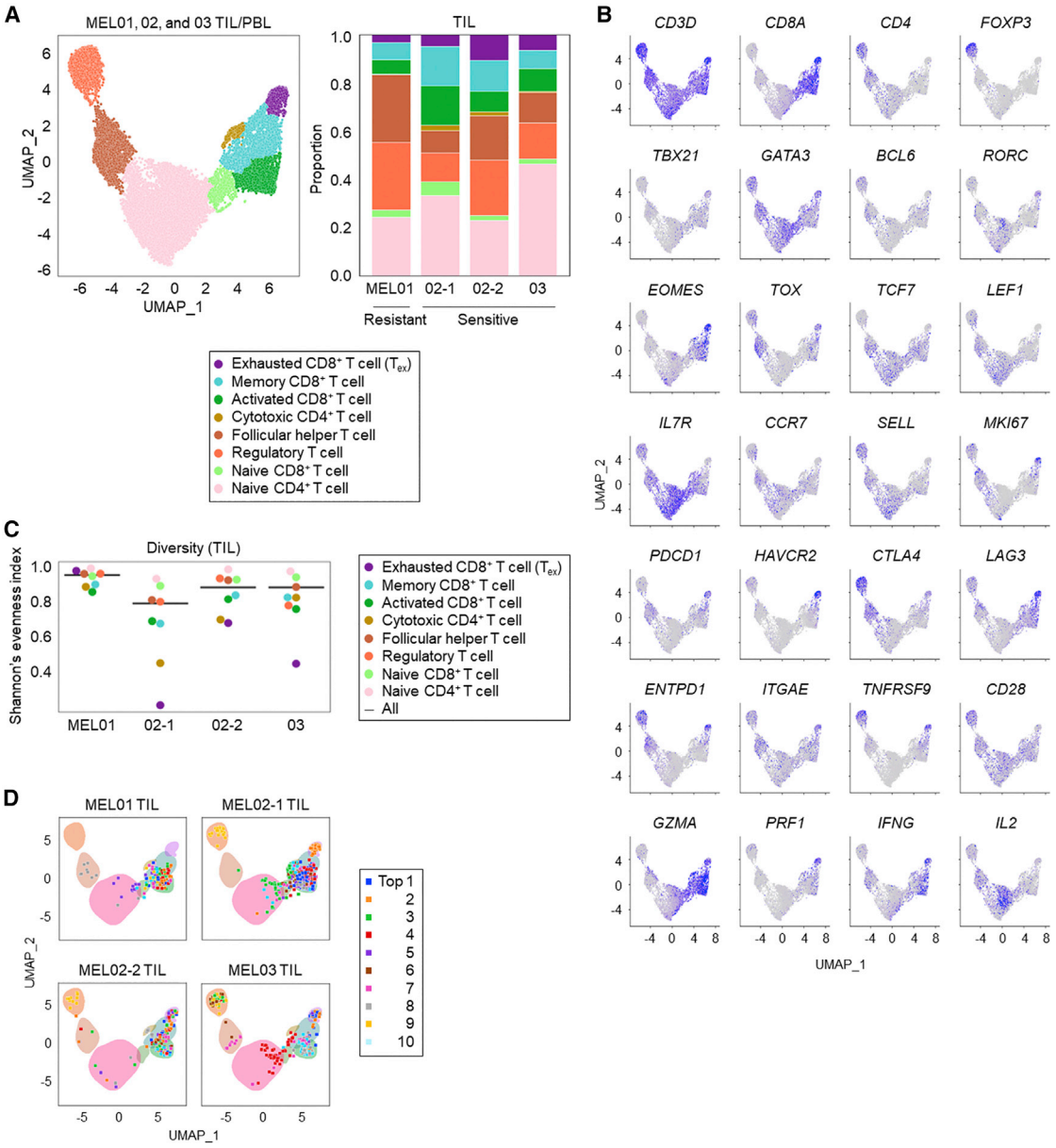

Figure 1. Skewed T cell clonotypes of tumor-infiltrating T cells were classified into both T_{ex} and $T_{non\text{-}ex}$ clusters

(A) Clustering of T cells from melanoma patients. Four tumor samples were digested to extract TILs. Sorted $CD3^+$ T cells from TILs and PBLs were analyzed with single-cell sequencing. Merged data of four TIL and two PBL samples were clustered using gene expression. UMAP figure (left) and the summary of TILs (right) are shown.

(B) Representative gene expression in each cluster. Representative genes that are frequently used for annotation are presented.

(C) Diversity of T cell clonotypes. The Shannon evenness indexes of each sample and each cluster are summarized.

(D) Distribution of the top 10 clonotypes in each TIL sample. The distribution of the top 10 clonotypes from each TIL sample in the UMAP figure is shown.

See also Figures S1 and S2; Tables S1, S2, and S3.

specific. In sharp contrast, the clonotype from clone #01 was hardly found in this UMAP figure, suggesting that tumor-specific T cells were scarcely detected in the TME from the patient with acquired resistance due to the loss of *B2M* (Figure 2C).

When we explored the top 10 skewed clonotypes from MEL02-1, only two clonotypes belonged to the T_{ex} cluster, while the others belonged to the $T_{non\text{-}ex}$ clusters, including activated $CD8^+$ T cells, memory $CD8^+$ T cells, and regulatory T cell clusters (Figure 1D). To further address the tumor specificity of these clonotypes, NFAT-luciferase reporter Jurkat cell lines transduced with each TCR (NFAT-Jurkat cell line) were developed from skewed T cell clonotypes in MEL02-1 cells and cocultured with the autologous tumor cell line (Figure S3B). The top 8 skewed TCRs against which antibodies were commercially available

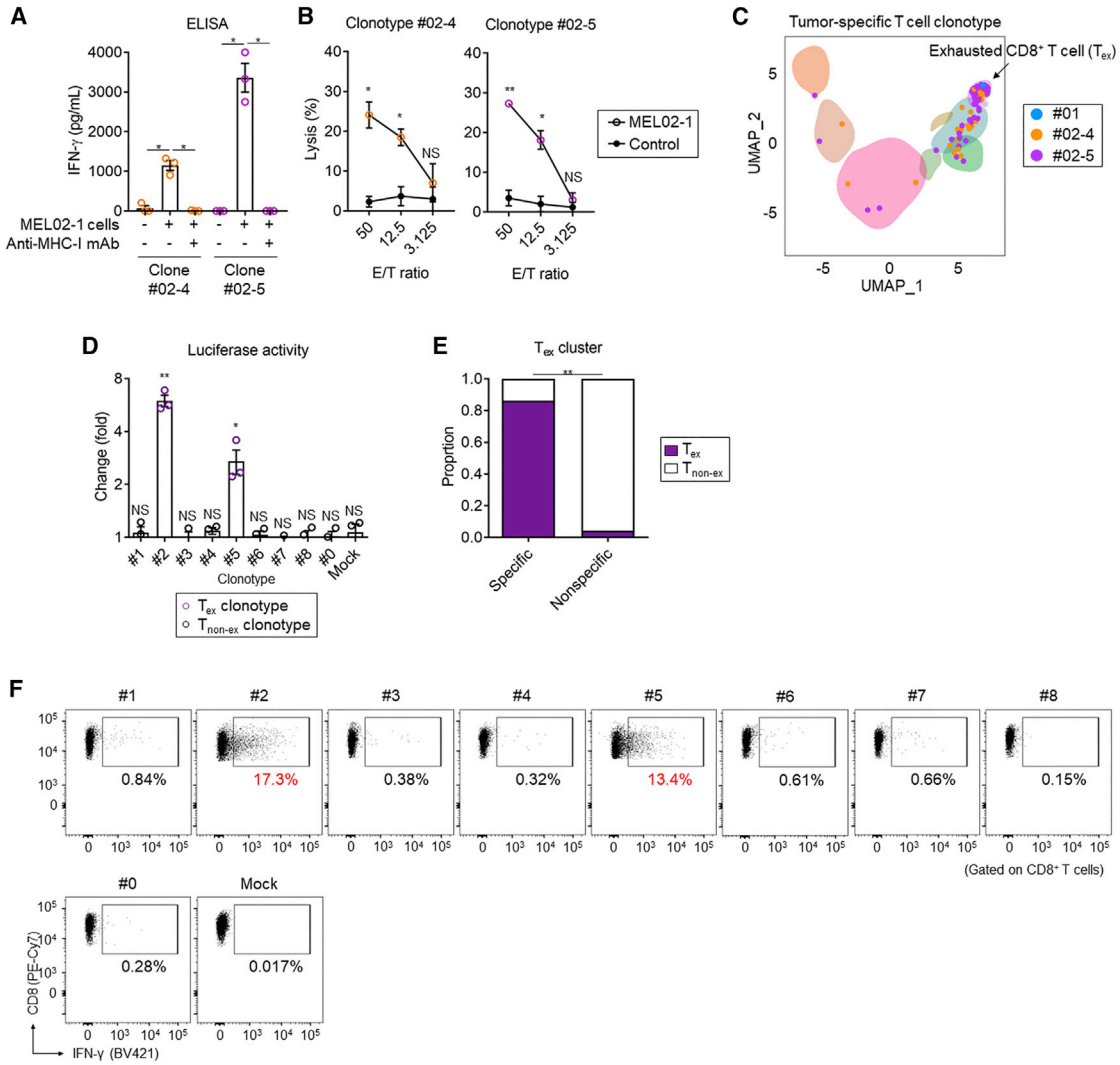

Figure 2. Among skewed clonotypes, those in the T_{ex}, but not the $T_{non\text{-}ex}$, cluster from the TME are tumor specific

(A) IFN-γ release assay of enriched clones from MEL02-1 TILs. After coculture with the autologous tumor cell line, the IFN-γ concentrations in the supernatants were analyzed with ELISA. For the negative control, an anti-MHC class I (MHC-I) mAb was added.

(B) Killing assay of enriched clones from MEL02. Calcein-AM-labeled tumor cells (target cells; T) were cocultured with each T cell clone (effector cells; E) at the indicated E/T ratios and then centrifuged. At 3 h of incubation, fluorescence was measured. The *B2M*-transduced MEL01 cell line was used as a negative control (Inozume et al., 2019).

(C) Distribution of the clonotypes from tumor-specific clones in MEL02. The TCRα and TCRβ chain V regions of enriched clones from MEL01 (#01) and MEL02-1 (#02-4 and #02-5) TILs were analyzed with the 5′ RACE method, and the clonotypes are highlighted in the UMAP figure.

(D) Tumor specificity of each clonotype in MEL02. Each TCR-transduced NFAT-Jurkat cell line was cocultured with an autologous tumor cell line. Luciferase activity was analyzed after 24 h of coculture. The top 8 skewed TCRs against which antibodies were commercially available were selected among cytotoxic T cell clonotypes from MEL02-1 TILs (#1 to #8). We compared the data with those from experiments without autologous tumor cell lines for statistical analyses. The fold change in each NFAT-Jurkat cell line without an autologous tumor cell line is presented. T_{ex} clonotypes were defined as those from which more than 20% of the T cells were classified as T_{ex}. Control clonotype #0 was selected from among the minor clonotypes in the TME that were frequently found in MHC-matched adaptive PBL datasets (Emerson et al., 2017).

(E) Comparison of the proportion of T_{ex} clones between tumor-specific and nonspecific T cells. We used the top 8 skewed clonotypes that were tested in (D) (#2 and #5, tumor specific versus #1, #3, #4, #6, #7, and #8, nonspecific).

(F) Representative flow cytometry staining of IFN-γ production. Each TCR-transduced $CD8^+$ T cells were analyzed with flow cytometry after 24 h of coculture with the autologous tumor cell line.

All *in vitro* experiments were performed in triplicate, and the means and SEMs are shown. One-way ANOVA tests with Bonferroni corrections were used in (A), paired t tests were used in (B and D), and Fisher's exact test was used in (E) to calculate statistical significance. *$p < 0.05$, **$p < 0.01$; NS, not significant.

See also Figures S1 and S3; Tables S1 and S4.

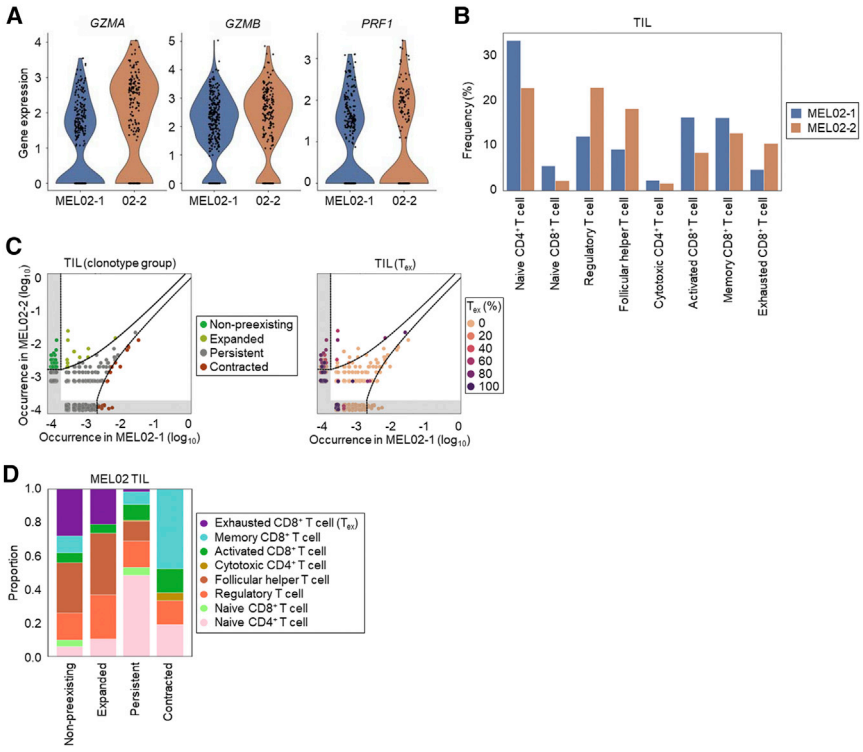

Figure 3. T cell clonotypes in the TME change dynamically after PD-1 blockade therapy

(A) Gene expression related to cytotoxicity in the T_{ex} cluster after PD-1 blockade. Each T cell was classified according to its gene expression, and violin plots of *GZMA*, *GZMB*, and *PRF1* expression in the T_{ex} clusters from MEL02-1 (pretreatment) and MEL02-2 (posttreatment) TILs are shown.

(B) T cell cluster change after PD-1 blockade. The comparison of T cell cluster frequencies between MEL02-1 and MEL02-2 TILs is shown.

(C) Clonotype change after PD-1 blockade. We merged the clonotypes of MEL02-2 TILs with those of MEL02-1 TILs, which were grouped into non-preexisting, expanded, persistent, or contracted clonotypes according to their frequencies in the TME. The clonotype groups (left) and frequencies of T_{ex} (right) are shown.

(D) The proportions of T cell clusters in the TME. The summary according to the clonotype groups (non-preexisting, expanded, persistent, and contracted) is shown.

See also Figure S1 and Table S1.

were selected among cytotoxic T cell clonotypes from MEL02-1 TILs (#1 to #8) (Table S4; Figure S3C). The luciferase activities of the two clonotypes (#2 and #5) from the T_{ex} clusters, which were the same TCR clonotype as clones #02-5 and #02-4, respectively (Table S4), were significantly increased after coculture with the autologous tumor cell line, meaning that these two clonotypes were tumor specific (Figure 2D). In contrast, the luciferase activities of the other six $T_{non\text{-}ex}$ clonotypes were comparable during culture, suggesting that they were not tumor specific (Figure 2D). These tumor-specific clones (#2 and #5) were dominantly classified into the T_{ex} cluster, as opposed to the nonspecific clones (#1, #3, #4, #6, #7, and #8) (224/260 versus 28/659, $p < 0.01$) (Figure 2E). Indeed, primary $CD8^+$ T cells transduced with T_{ex} TCRs but not $T_{non\text{-}ex}$ TCRs produced IFN-γ and had high CD69 expression after coculture with the autologous tumor cell line (Figures 2F and S3D). Similarly, we confirmed that T_{ex} clonotypes in MEL03 TILs were tumor specific using the same luciferase assays (Figure S3E; Table S4). In line with Simoni et al. (2018), Scheper et al. (2019), and Oliveira et al. (2021), these findings indicate that tumor-infiltrating T cells include both tumor-specific and nonspecific T cells with skewed clonotypes and that the clonotypes in the T_{ex} cluster are tumor specific.

Preexisting clonotypes in the T_{ex} cluster expand, and other clonotypes appear in the TME after PD-1 blockade in a superresponder

To elucidate the impact of PD-1 blockade therapy on the TME, samples collected before and after PD-1 blockade (MEL02-1 and MEL02-2, respectively) were compared. Within the T_{ex} clonotypes, the expression of genes associated with cytolytic activity was increased from MEL02-1 to MEL02-2 (Figure 3A). In addition, the T_{ex} cluster became abundant in the TME (Figure 3B). Follicular helper T (T_{fh}) cell and T_{reg} cell clusters also increased after PD-1 blockade (Figure 3B), as was previously observed (Bassez et al., 2021; Yost et al., 2019).

We next merged clonotypes of MEL02-2 TILs with MEL02-1 TILs. The clonotypes were classified into four groups: non-preexisting, expanded, persistent, and contracted (Figure 3C). T_{ex} clonotypes were mainly detected in the non-preexisting and expanded groups and scarcely detected in the persistent group or in the contracted group (Figures 3C and 3D). These findings are consistent with previous studies (Bassez et al., 2021; Sade-Feldman et al., 2018; Yost et al., 2019), suggesting that PD-1 blockade promotes tumor-specific T cell clonal changes through expansion and infiltration of fresh T cell clonotypes, in addition to reinvigoration of preexisting clonotypes.

PD-1 blockade promotes clonal expansion and infiltration of T_{ex}

A dynamic clonal change in the T_{ex} cluster could be induced by antigenic alteration of cancer cells during treatment, as suggested by a previous study showing antigenic changes after PD-1 blockade (Anagnostou et al., 2017). Thus, we investigated whether each clonotype could respond to autologous tumor cell lines derived from pretreatment (MEL02-1) and posttreatment (MEL02-2) samples using the NFAT-Jurkat cell line (Tables S4 and S5). The top 8 skewed TCRs against which antibodies were commercially available were selected among cytotoxic T cell clonotypes from MEL02-2 TILs (#9 to #16) (Tables S4 and S5; Figure S4A). All clonotypes in the T_{ex} cluster responded to both cell lines, even if they were classified into the non-preexisting group (Figure 4A). In contrast, no clonotype in $T_{non\text{-}ex}$

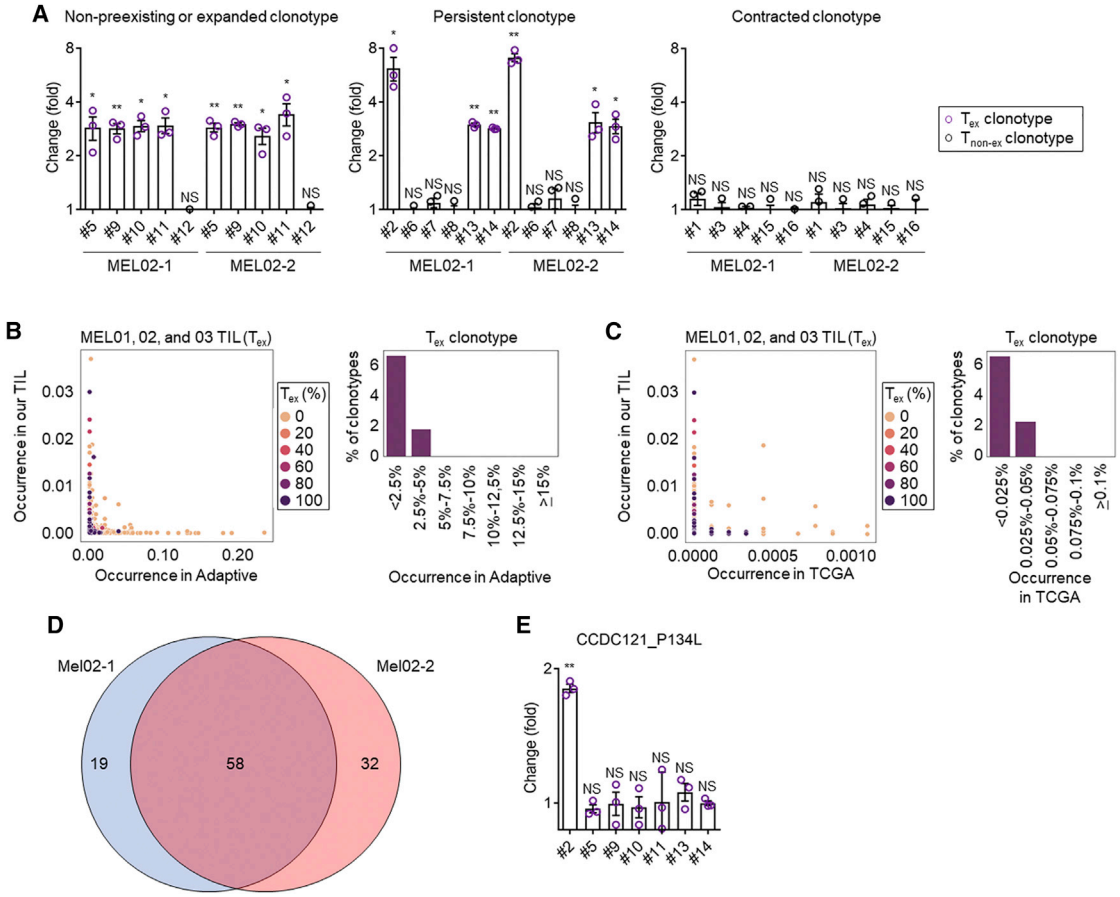

Figure 4. T cell clonotypes in the T_{ex} cluster respond to both pretreatment and posttreatment tumor cell lines, which recognize neoantigens

(A) Tumor specificity of each clonotype. Tumor specificity was analyzed as described in Figure S3B. The fold change in luciferase activity in each NFAT-Jurkat cell line without autologous tumor cell lines was calculated. The top 8 skewed TCRs against which antibodies were commercially available were selected among cytotoxic T cell clonotypes ($CD8^+$ or cytotoxic $CD4^+$ T cells) from MEL02-2 TILs (#9 to #16). T_{ex} clonotypes were defined as those in which more than 20% of the T cells were classified as T_{ex}.

(B and C) The comparison between our own TIL data and public datasets of TCR sequences. We used adaptive PBL data (Emerson et al., 2017) in an MHC-matching manner (B) and TCGA data (Li et al., 2016) in an MHC-nonmatching manner (C). Merged figures with public data based on CDR3 sequences (left) and the occurrence of the T_{ex} clonotype of our own TILs in public data (right) are shown.

(D) Venn diagram of nonsynonymous somatic mutations. Whole-exome sequencing of MEL02-1 and MEL02-2 cell lines was performed. The numbers of nonsynonymous somatic mutations are shown.

(E) Peptide assay. Seven TCR-transduced NFAT-Jurkat cell lines that responded to autologous tumor cell lines were cocultured with irradiated autologous cells after CCDC121_P134L peptide pulse. Luciferase activity was analyzed after 24 h of coculture. The fold change in each NFAT-Jurkat cell line with wild-type peptide pulses is shown, and we compared it with wild-type pulse data for statistical analyses.

All *in vitro* experiments were performed in triplicate, and the means and SEMs are shown. Paired t tests were used to calculate statistical significance in (A and E). $^*p < 0.05$, $^{**}p < 0.01$; NS, not significant.

See also Figures S1 and S4; Tables S1, S4, S5, and S6.

clusters, regardless of group, responded to the autologous tumor cell lines (Figure 4A). Therefore, dynamic tumor-specific clonal changes after PD-1 blockade, especially expansion and infiltration, are caused by PD-1 blockade but not antigenic alteration of cancer cells.

The comparison between our own TIL data and public datasets of TCR sequences from MHC-matched peripheral blood lymphocytes (PBLs) and TCGA datasets revealed that the T_{ex} clonotypes detected in our study were rarely detected in any public datasets (Emerson et al., 2017; Li et al., 2016) (Figures 4B and 4C). These findings prompted us to investigate whether tumor-specific clonotypes in the T_{ex} cluster in our study recognized unique cancer antigens derived from somatic mutations (neoantigens) (Rizvi et al., 2015). Although a significant clonal change was observed in cancer cells from MEL02-1 to MEL02-2 after PD-1 blockade, more than half of the somatic mutations overlapped (Figures 4D and S4B). We then predicted neoantigen candidates with strong binding using NetMHCpan version 4.0 (%Rank $\leq$0.5) (Hoof et al., 2009; Jurtz et al., 2017) from the overlapping somatic mutations because the T_{ex} clonotypes responded to the autologous tumor cell lines from both the pretreatment and posttreatment samples (Table S6). In addition,

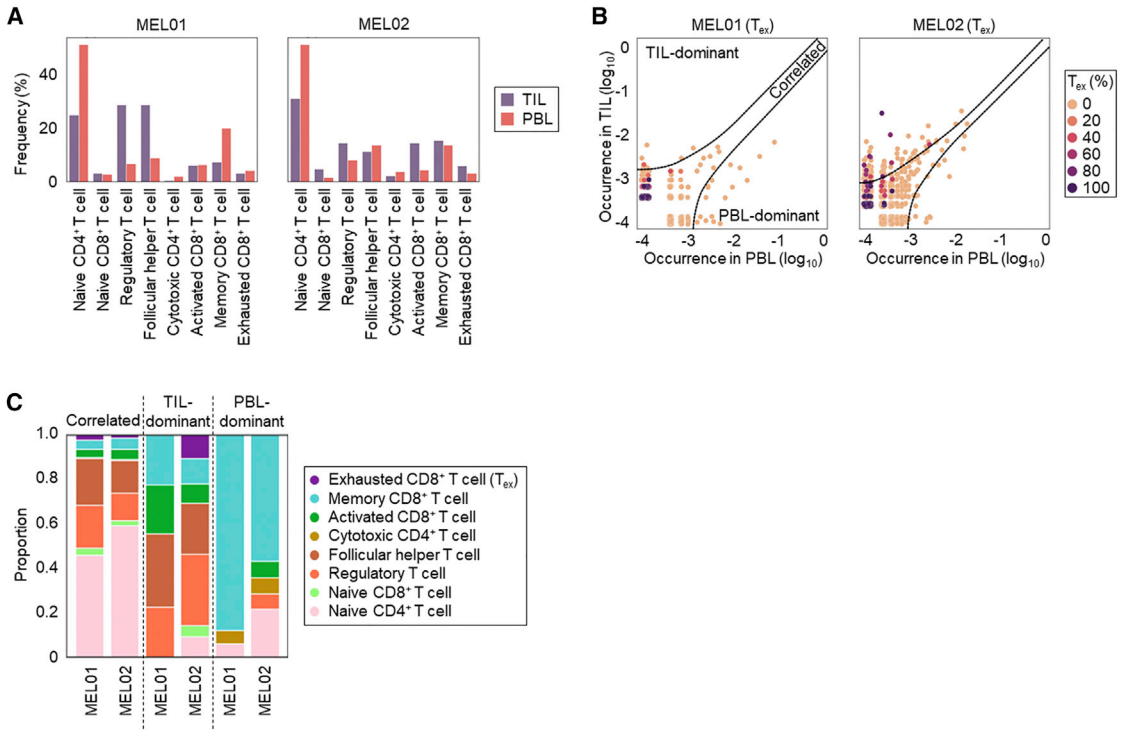

Figure 5. Peripheral blood has few T_{ex} clonotypes

(A) The comparison of cluster frequencies between TILs and PBLs. The frequency of each cluster in each sample (MEL01 TIL/PBL and 02 TIL/PBL) is shown.

(B) The comparison of clonotypes between TILs and PBLs. We merged the PBL clonotypes and TIL clonotypes in each patient and then classified them as correlated, TIL dominant, or PBL dominant according to their frequencies. Merged figures are shown.

(C) The proportions of T cell clusters. T cell cluster proportions according to the clonotype group (correlated, TIL dominant, and PBL dominant) in each patient are shown.

See also Figures S1 and S5; Table S1.

cancer/testis (CT) antigens including Melan A/MART-1 and gp100 were also evaluated using representative well-known peptides (Melan A/MART-1, ELAGIGILTV; gp100, YLEPGPVTA) and predicted peptides by NetMHCpan version 4.0 (Table S6). We evaluated the fold changes of mutated to wild-type peptides for neoantigens, or peptide-pulsed to nonpulsed conditions for CT antigens, respectively. Among all tested peptides, a T_{ex} clonotype (#2) responded to a unique peptide derived from CCDC121_P134L (Figures 4E, S4C, and S4D).

Few T_{ex} clonotypes are found in the peripheral blood

We next compared these TIL data with PBL data. The naive $CD4^+$ T cell cluster was dominant in PBLs, and significant differences in the frequency of each cluster were observed between TILs and PBLs in MEL01 and MEL02 (Figures 5A and S2B). T cell clonotypes were merged in each patient, and three groups of clonotypes were developed: correlated, TIL-dominant, and PBL-dominant groups (Figure 5B). T_{ex} clonotypes were highly detected in the TIL-dominant group of MEL02, and few T_{ex} clonotypes coincided in TILs and PBLs (Figures 5B and 5C). In addition, the correlated and PBL-dominant groups mostly consisted of clonotypes in $T_{non\text{-}ex}$ clusters (Figures 5B and 5C). Clonotypes in $T_{non\text{-}ex}$ clusters that were considerably (more than 1% [#1 and #3]) skewed in both TILs and PBLs did not respond to the autologous tumor cell lines (Figure 4A; Table S5), meaning that these clonotypes are not tumor specific. These findings suggest that few tumor-specific T cell clonotypes are found in peripheral blood, although tumor nonspecifically skewed clonotypes in $T_{non\text{-}ex}$ clusters are significantly detected in both TILs and PBLs, in accordance with previous studies (Wu et al., 2020; Yost et al., 2019) (Figure S5).

TDLNs contain a significant number of T_{ex}

Recent studies showing that TDLNs retain T_{ex} in mouse models (Dammeijer et al., 2020; Francis et al., 2020) and that shared TCRs between tumor tissues and TDLNs in neoantigen-rich cancer types (Inamori et al., 2021) prompted us to investigate TDLNs in human clinical samples. We collected paired samples of TILs, TDLN lymphocytes (LNLs), and PBLs from three cancer patients (two lung cancers and one head and neck cancer) (Table S1). Dissected TDLNs were cut in half at the maximum circumference, and one-half was submitted to pathological examination. The remaining halves of those TDLNs that were pathologically diagnosed as nonmetastatic LNs were subjected to further analyses. These paired samples were analyzed with both droplet-based 5′ scRNA-seq and scTCR-seq. In total, we obtained paired TCR sequences from 61,220 out of 77,952 T cells (78.5%, Table S2). The T cells were classified into seven clusters

based on gene expression profiling (Figures 6A, 6B, and S6; Table S7) (Yost et al., 2019). Considerable amounts of T cells in LNLs were classified into the naive, T_{fh}, and T_{reg} cell clusters, whereas T cells in TILs were overwhelmingly classified into the T_{ex} cluster (Figures 6A, 6B, and S6). A considerable number of T_{ex} cells in TILs, which could be tumor specific, were found in LNLs, although they were rarely detected in PBLs (Figure 6C). Interestingly, many such clonotypes in LNLs were also mainly classified into T_{ex} clusters, whereas most $T_{non\text{-}ex}$ clonotypes of TILs were classified into $T_{non\text{-}ex}$ clusters in LNLs (52/73 versus 1/82, $p < 0.01$) (Figures 6D, 6E, and S6C). In summary, TDLNs contain a considerable number of T_{ex} clonotypes, which can be tumor-specific T cells.

PD-1 blockade promotes infiltration of T_{ex} clonotypes into the TME from TDLNs in mouse models

Next, we validated our human data with *in vivo* mouse models treated with or without FTY720, which locks lymphocytes in LNs (Figure 7A). To this end, we employed MC-38/OVA and E.G7 as PD-1 blockade-sensitive tumor models and B16F10 as a PD-1 blockade-resistant tumor model (Figures 7B and S7A). PD-1 expression by $CD8^+$ T cells in the TME significantly increased after PD-1 blockade in PD-1 blockade-sensitive tumor models, whereas it was comparable in a PD-1 blockade-resistant tumor model (Figures 7C and S7). We next analyzed the TCR repertoire of PD-1^+CD8^+ T cells (T_{ex}) in the TME of a PD-1 blockade-sensitive MC-38/OVA tumor model. Non-pre-existing PD-1^+CD8^+ T cell clonotypes tended to infiltrate into the TME after PD-1 blockade, leading to higher diversity of the TCR repertoire in PD-1^+CD8^+ T cells (Figure 7D). In contrast, FTY720 diminished the effectiveness of PD-1 blockade in PD-1 blockade-sensitive tumor models (Figure 7B). Accordingly, PD-1 expression by $CD8^+$ T cells in the TME significantly decreased and did not increase after PD-1 blockade under the treatment with FTY720 (Figure 7C). These results were consistent with our findings in human clinical samples, supporting the importance of infiltration of tumor-specific T_{ex} clonotypes from TDLNs in PD-1 blockade-mediated antitumor immunity.

DISCUSSION

PD-1 blockade provides a remarkable clinical response in multiple cancer types, whereas efficacy is otherwise unsatisfactory (Borghaei et al., 2015; Brahmer et al., 2015; Hodi et al., 2010; Larkin et al., 2015; Topalian et al., 2015; Zou et al., 2016). PD-1 blockade reportedly reinvigorates tumor-specific T cells in the TME, leading to tumor regression (Topalian et al., 2015; Zou et al., 2016). Nevertheless, not all tumor-infiltrating T cells are tumor specific, and they include nonspecific bystander T cells (Oliveira et al., 2021; Scheper et al., 2019; Simoni et al., 2018), indicating the importance of identifying the critical fraction(s) that are essential for tumor regression. Several studies have revealed that clonally skewed T cells in the TME can be tumor specific and that the T cell population expresses T cell exhaustion-associated signature molecules, such as PD-1, 4-1BB, CD39, and CD103 (Gros et al., 2014; Li et al., 2019; Tirosh et al., 2016; Tumeh et al., 2014). However, these previous studies have neglected a critical aspect of T cell responses in antitumor immunity: the tumor specificity has not been fully addressed. Here, we show detailed scRNA-seq and scTCR-seq analyses of tumor-infiltrating T cells from melanoma patients. Considerable amounts of clonally skewed T cells were observed in the TME. However, these skewed clonotypes include both T_{ex} and $T_{non\text{-}ex}$ clusters. Tumor-specific T cells were detected solely in clonotypes in the T_{ex} cluster using autologous tumor cell lines. In contrast, T cells in $T_{non\text{-}ex}$ clusters were not tumor specific even though they harbored skewed clonotypes in the TME. These are consistent with a recent study (Oliveira et al., 2021). Overall, many skewed clonotypes in the T_{ex} cluster are tumor (neoantigen) specific, suggesting that we can identify tumor-specific T cell clonotypes by combination with clonal skewing and immune profiling; therefore, immune monitoring can be focused on these populations as effective antitumor immunity.

A dynamic change (clonal expansion and infiltration of the T_{ex} cluster) in the T_{ex} clonotypes upon PD-1 blockade was demonstrated in accordance with previous studies (Bassez et al., 2021; Yost et al., 2019). However, it remains unclear whether it is antigenic changes in tumor cells due to genetic alterations that occur during PD-1 blockade or the PD-1 blockade by itself that causes the dynamic clonal changes. We clearly show that PD-1 blockade intrinsically induces dynamic clonal changes. Although the T_{ex} clonotypes were changed after PD-1 blockade, all clonotypes in the T_{ex} cluster responded to both pretreatment and posttreatment tumor cell lines. In addition, T_{fh} cell and T_{reg} cell clusters also increased after PD-1 blockade, as was previously observed (Bassez et al., 2021; Yost et al., 2019). T_{fh} cells induce maturation of B cells and reportedly have high PD-1 expression, which is consistent with proliferation of these cells after PD-1 blockade (Crotty, 2019). Accordingly, recent studies have demonstrated that tumor-infiltrating T_{fh} cells and B cells play important roles in antitumor immunity (Cabrita et al., 2020; Helmink et al., 2020; Hollern et al., 2019; Niogret et al., 2021; Petitprez et al., 2020). We previously showed that tumor-infiltrating T_{reg} cells also had high PD-1 expression and that PD-1^+ T_{reg} cells in the TME were increased by PD-1 blockade, contributing to resistance to PD-1 blockade (Kamada et al., 2019; Kumagai et al., 2020a; Togashi et al., 2019). Our present scRNA-seq data are consistent with our previous studies, strongly suggesting that such PD-1^+ T_{reg} cells are a therapeutic candidate for cancer immunotherapy.

Based on our present and recent studies (Bassez et al., 2021; Yost et al., 2019), one essential question is raised: where do the tumor-specific clonotypes in the T_{ex} cluster infiltrate from? It is envisioned that such clonotypes may be derived from the periphery. However, very few tumor-specific clonotypes overlapped between TILs and PBLs. Previous studies also showed that such clonotypes in the T_{ex} cluster of TILs rarely overlapped with PBLs (Wu et al., 2020; Yost et al., 2019). Since T cells are primed by antigen-presenting cells that capture tumor antigens in tumor tissues and infiltrate into TDLNs (Chen and Mellman, 2013; Förster et al., 2012), TDLNs may be a primary source of newly infiltrating tumor-specific clonotypes in the T_{ex} cluster promoted by PD-1 blockade. Indeed, recent studies have revealed that T cells in TDLNs are enriched for tumor-specific T cells in

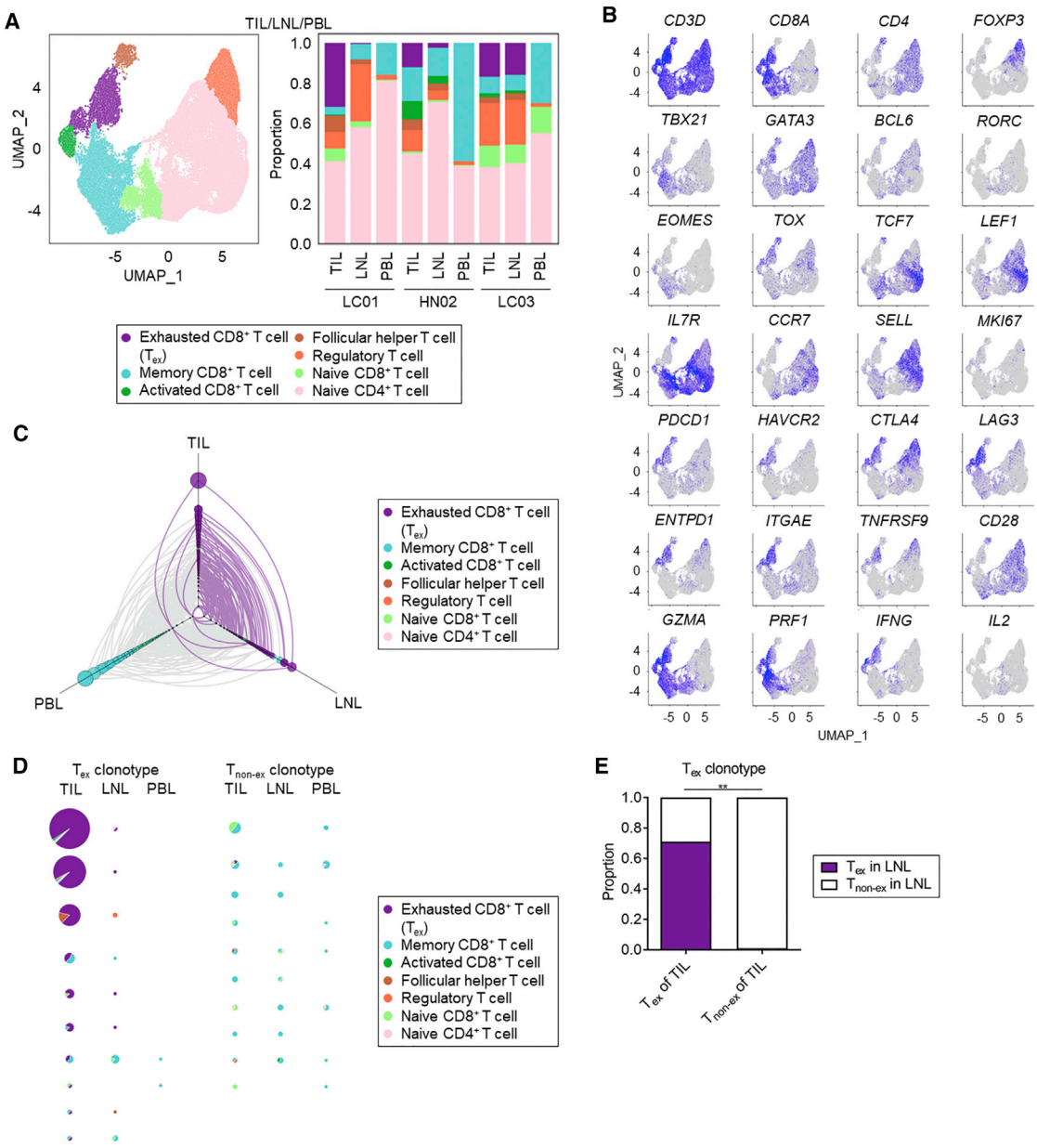

Figure 6. TDLNs have considerable tumor-specific T cell clonotypes

(A) Clustering of T cells from LC01, HN02, and LC03. Three tumor samples and three TDLN samples from the patients (LC01 and LC03, lung adenocarcinoma; HN02, head and neck squamous cell carcinoma) were digested to extract TILs and LNLs, respectively. Sorted $CD3^+$ T cells from TILs, LNLs, and PBLs were analyzed with single-cell sequencing. Merged data for three TIL, three LNL, and three PBL samples were clustered using gene expression. UMAP figure (left) and the summary (right) are shown.

(B) Representative gene expression in each cluster. Representative genes that are frequently used for annotation are presented.

(C) The comparison of T cell clonotypes among TILs, LNLs, and PBLs from three patients. Overlapping clonotypes at each site are connected by lines; purple lines indicate T_{ex} clonotypes of TILs, and the circle size indicates the frequency of clonotype in each sample. T_{ex} clonotypes were defined as those in which more than 20% of the T cells were classified as T_{ex}.

(D) Clusters belonging to overlapping T cell clonotypes. We selected the top 10 overlapping T_{ex} (left) or $T_{non\text{-}ex}$ (right) clonotypes of TILs among $CD8^+$ T cells from LC01.

(E) The proportion of T_{ex} clonotypes in LNLs among overlapping $CD8^+$ T cell clonotypes with TILs. The comparison between T_{ex} and $T_{non\text{-}ex}$ clonotypes of TILs from three patients is shown.

Fisher's exact test was used to calculate statistical significance in (E). $^{**}p < 0.01$.

See also Figure S6; Tables S1, S2, and S7.

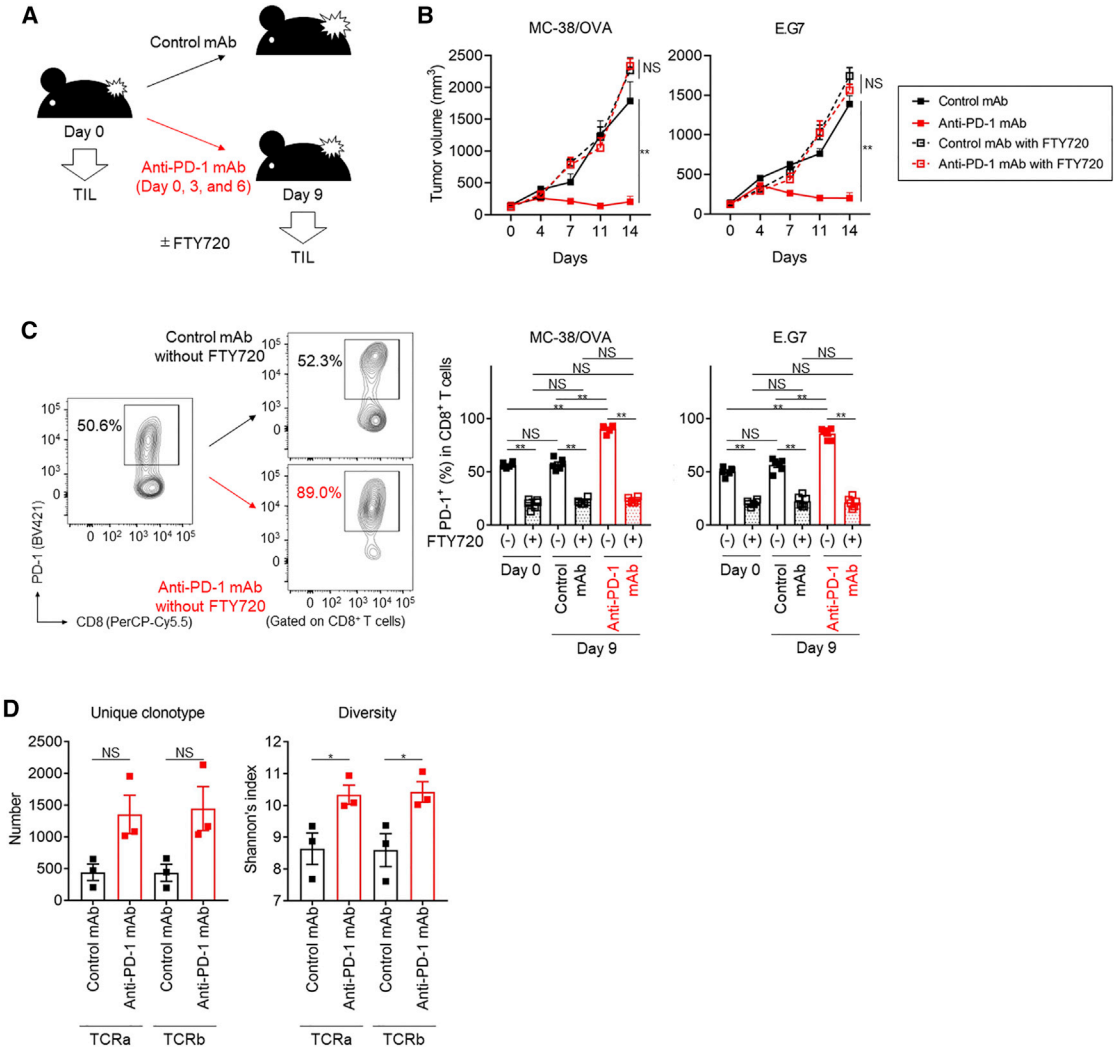

Figure 7. T_{ex} and its TCR diversity increase in the TME of mouse PD-1-sensitive tumor models after PD-1 blockade

(A) Graphic of the experimental schema of *in vivo* experiments. TILs were extracted at baseline and at 10 days after initiation of treatment with or without FTY720 and were subjected to analyses.

(B) Tumor growth of each tumor model. Cells (1×10^6) were injected subcutaneously, and tumor volume was monitored twice a week. Mice were grouped when the tumor volume reached approximately 100 mm^3 (n = 6 per group), after which anti-PD-1 mAb or control mAb was administered intraperitoneally three times at intervals of 3 days, and FTY720 was administered intraperitoneally every day.

(C) PD-1 expression by $CD8^+$ T cells in the TME. Representative flow cytometry staining (left) and summaries (right) are shown.

(D) TCR unique clonotype numbers (left) and diversities (right) in tumor-infiltrating PD-1^+CD8^+ T cells. Sorted PD-1^+CD8^+ T cells from TILs that were extracted as described in (A) were sequenced. Shannon's index was calculated to evaluate diversity.

All *in vivo* experiments were performed in duplicate and produced similar results in both cases; the means and SEMs are shown. Two-way ANOVA, one-way ANOVA with Bonferroni correction, and t tests were used to calculate statistical significance in (B, C, and D), respectively. *$p < 0.05$, **$p < 0.01$; NS, not significant. See also Figure S7.

mouse models (Dammeijer et al., 2020; Francis et al., 2020). In these models, tumor-specific T cells express PD-1 in TDLNs. Furthermore, we recently showed significantly shared TCRs between tumor tissues and TDLNs in neoantigen-rich cancer types compared with PBLs or neoantigen-poor cancer types (Inamori et al., 2021). Following these previous studies, we have shown that TDLNs in human clinical samples have a considerable number of tumor-specific T cell clonotypes and that such clonotypes exhibit the exhausted phenotype. In addition, FTY720, which locks lymphocytes in LNs, diminished the efficacy of PD-1 blockade, significantly decreased PD-1^+CD8^+ T cells in the TME, and abrogated the increased PD-1^+CD8^+ T cells in the TME after PD-1 blockade, suggesting infiltration of tumor-specific T cell clonotypes from TDLNs and its importance in anti-tumor immunity.

Since we do not always have the opportunity to access tumor tissues, peripheral blood is useful in clinical settings. However, we found few of the tumor-specific T cell clonotypes that were

found in TILs as tumor-specific clonotypes in the T_{ex} cluster in PBLs. In addition, the clonotypes that were shared between TILs and PBLs were mostly tumor-nonspecific clonotypes in $T_{non\text{-}ex}$ clusters, in accordance with previous studies (Wu et al., 2020; Yost et al., 2019). Our findings indicate that such clonotypes are expanded in TILs and LNLs but rarely expanded in PBLs. Such T cell clonotypes can be recruited into the TME through blood from TDLNs. However, it can be difficult to detect such few clonotypes due to several limitations including technical limitations. Indeed, we recently showed significantly shared TCR repertoires between tumor tissues and TDLNs compared with PBLs (Inamori et al., 2021). While a previous study revealed that PD-1^+CD8^+ T cells in PBLs could be tumor and neoantigen specific (Gros et al., 2016), it may be difficult to identify all tumor-specific clonotypes from PBLs.

In summary, we found that tumor-infiltrating T cells comprised skewed clonotypes in both T_{ex} and $T_{non\text{-}ex}$ clusters. Among them, clonotypes in the T_{ex}, but not those in the $T_{non\text{-}ex}$, cluster were tumor and neoantigen specific. After PD-1 blockade, preexisting tumor-specific T cell clonotypes were expanded, and other such T cell clonotypes also infiltrated the TME. The increased T_{ex} and infiltration promoted by PD-1 blockade was also observed in mouse models. We also showed that TDLNs had a considerable number of T_{ex} clonotypes, which can be the origin of clonotype infiltration promoted by PD-1 blockade. Therefore, PD-1 blockade not only reinvigorates tumor-specific T cells in the T_{ex} cluster but also promotes expansion and infiltration of tumor-specific T cell clonotypes, which can play an important role in PD-1 blockade-mediated antitumor immunity.

Limitations of the study

One of limitations is the limited patient population. However, similar findings, such as increased T_{ex} clusters and infiltration of non-preexisting T_{ex} clonotypes, were also observed in other studies and our PD-1 blockade-sensitive mouse tumor models (Bassez et al., 2021; Yost et al., 2019). Furthermore, FTY720 diminished the efficacy of PD-1 blockade, significantly decreased PD-1^+CD8^+ T cells in the TME, and abrogated the increased PD-1^+CD8^+ T cells in the TME after PD-1 blockade in our PD-1 blockade-sensitive mouse tumor models. Thus, we propose that PD-1 blockade promotes tumor-specific clonal expansion in the T_{ex} cluster and infiltration from TDLNs for effective antitumor immunity. While our data reveal the appearance of non-preexisting tumor-specific clonotypes, this finding could be due to technical limitations. We analyzed fewer than 1×10^4 T cells in each sample and there was an approximately 20% dropout in scTCR-seq, suggesting not enough cells to find such rare clonotypes. Intratumoral heterogeneity could also induce a sampling problem. Thus, it cannot be excluded that "non-preexisting" clones are clones that simply were not sampled in the tumor samples.

There are some concerns about the resolution of scRNA-seq gene expression data (Stoeckius et al., 2017). The problems of resolution may responsible for the many naive $CD4^+$ T cells in our scRNA-seq data. To resolve this problem, CITE-seq using oligonucleotide-conjugated antibodies can help us (Stoeckius et al., 2017).

STAR★METHODS

Detailed methods are provided in the online version of this paper and include the following:

- KEY RESOURCES TABLE
- RESOURCE AVAILABILITY
  - Lead contact
  - Materials availability
  - Data and code availability
- EXPERIMENTAL MODEL AND SUBJECT DETAILS
  - Patients and samples
  - Cell lines
  - *In vivo* animal models
- METHOD DETAILS
  - Immunohistochemistry
  - scRNA-seq and scTCR-seq
  - Data analysis for single cell sequencing
  - *In vitro* expansion of TILs
  - Enrichment of tumor-specific T cell clones, cloning, and identification of TCR clonotypes
  - Constructs, virus production, and transfection
  - IFN-γ release assay
  - Killing assay
  - Luciferase reporter assay for tumor-specificity
  - Whole-exome sequencing
  - Transcriptome sequencing and expression analysis
  - Clonal analysis in tumor cells
  - Analyses of public datasets
  - Antigen prediction
  - Peptide assay
  - Mouse TCR sequencing and data analyses
  - Flow cytometry analyses
- QUANTIFICATION AND STATISTICAL ANALYSIS

SUPPLEMENTAL INFORMATION

Supplemental information can be found online at https://doi.org/10.1016/j.celrep.2022.110331.

ACKNOWLEDGMENTS

We thank Ms. Noriko Sakurai for their technical assistance.

This study was supported by Grants-in-Aid for Scientific Research (S grant no. 17H06162 to H.N., B grant no. 20H03694 to Y.T., and C grant no. 19K08744 to T.I.) from the Ministry of Education, Culture, Sports, Science and Technology of Japan; the Project for Cancer Research and Therapeutic Evolution (P-CREATE, nos. 16cm0106301h0002 to H.N., 18cm0106340h0001 to K.Y. and Y.T., 19cm0106502 to M.K., and 21cm0106383 to K.Y. and Y.T.); Practical Research for Innovative Cancer Control (19ck0106521h0001 to K.Y. and Y.T.); the Development of Technology for Patient Stratification Biomarker Discovery grant (no.19ae0101074s0401 to H.N.) from the Japan Agency for Medical Research and Development (AMED); the Fusion Oriented Research for disruptive Science and Technology (FOREST) (no. 21-211033868 to Y.T.) from Japan Science and Technology Agency (JST); the National Cancer Center Research and Development Fund (nos. 28-A-7 and 31-A-7 to H.N.); the Naito Foundation (to Y.T.); the Takeda Science Foundation (to Y.T.); the Mitsubishi Foundation (to Y.T.); the Tokyo Biochemical Research Foundation (to Y.T.); the Daiichi Sankyo Foundation (to Y.T.); the Foundation for Promotion of Cancer Research Japan (to Y.T.); the Mochida Memorial Foundation (to Y.T.); the Kanae Foundation for the

Promotion of Medical Science (to Y.T.); the Yasuda Memorial Foundation for Medicine (to Y.T.); the MSD Life Science Foundation (to Y.T.); the Kowa Life Science Foundation (to Y.T.); the Senri Life Science Foundation (to Y.T.); and the Uehara Memorial Foundation (to Y.T.). This study was partially supported by KOTAI Biotechnologies Inc.

AUTHOR CONTRIBUTIONS

Conceptualization, H.N. and Y.T.; methodology, J.N., T.I., N.S., R.A., M.I., K.Y., H.N., and Y.T.; investigation, J.N., T.I., N.S., R.A., M.I., K.Y., M.K., T.U., T.I., E.T., T.M., A.H., T.O., M.Y., T.I., K.K., K.S., T.H., V.K., T.K., H. Matsue, M.H., H. Mano, Y.S., H.N., and Y.T.; writing – original draft, J.N., T.I., N.S., K.Y., M.K., H.N., and Y.T.; writing – review & editing, J.N., T.I., N.S., K.Y., M.K., H.N., and Y.T.; funding acquisition, T.I., K.Y., M.K., H.N., and Y.T.

DECLARATION OF INTERESTS

N.S., M.I., and K.Y. are employees of KOTAI Biotechnologies Inc. T.I. received honoraria and research grants from Ono Pharmaceutical, Bristol-Myers Squibb, and MSD outside of this study. T.H. received a research grant from Ono Pharmaceutical outside of this study. H. Mano received a research grant from Ono Pharmaceutical outside of this study. H.N. received honoraria and research funding from Ono Pharmaceutical, Chugai Pharmaceutical, MSD and Bristol-Myers Squibb, and research funding from Taiho Pharmaceutical, Daiichi-Sankyo, Kyowa Kirin, Zenyaku Kogyo, Oncolys BioPharma, Debiopharm, Asahi-Kasei, Sysmex, Fujifilm, SRL, Astellas Pharmaceutical, Sumitomo Dainippon Pharma, and BD Japan outside of this study. Y.T. received a research grant from KOTAI Biotechnologies Inc. related to this study. Y.T. also received research grants and honoraria from Ono Pharmaceutical, Bristol-Myers Squibb, and Daiichi-Sankyo, and honoraria from AstraZeneca, Chugai Pharmaceutical, and MSD outside of this study. All other authors declare no competing interests.

Received: February 7, 2021
Revised: October 21, 2021
Accepted: January 11, 2022
Published: February 1, 2022

REFERENCES

Amaria, R.N., Reddy, S.M., Tawbi, H.A., Davies, M.A., Ross, M.I., Glitza, I.C., Cormier, J.N., Lewis, C., Hwu, W.J., Hanna, E., et al. (2018). Neoadjuvant immune checkpoint blockade in high-risk resectable melanoma. Nat. Med. *24*, 1649–1654. https://doi.org/10.1038/s41591-018-0197-1.

Anagnostou, V., Smith, K.N., Forde, P.M., Niknafs, N., Bhattacharya, R., White, J., Zhang, T., Adleff, V., Phallen, J., Wali, N., et al. (2017). Evolution of neoantigen landscape during immune checkpoint blockade in non-small cell lung cancer. Cancer Discov. *7*, 264–276. https://doi.org/10.1158/2159-8290.CD-16-0828.

Bassez, A., Vos, H., Van Dyck, L., Floris, G., Arijs, I., Desmedt, C., Boeckx, B., Vanden Bempt, M., Nevelsteen, I., Lambein, K., et al. (2021). A single-cell map of intratumoral changes during anti-PD1 treatment of patients with breast cancer. Nat. Med. *27*, 820–832. https://doi.org/10.1038/s41591-021-01323-8.

Blank, C.U., Haining, W.N., Held, W., Hogan, P.G., Kallies, A., Lugli, E., Lynn, R.C., Philip, M., Rao, A., Restifo, N.P., et al. (2019). Defining 'T cell exhaustion'. Nat. Rev. Immunol. *19*, 665–674. https://doi.org/10.1038/s41577-019-0221-9.

Bolotin, D.A., Poslavsky, S., Mitrophanov, I., Shugay, M., Mamedov, I.Z., Putintseva, E.V., and Chudakov, D.M. (2015). MiXCR: software for comprehensive adaptive immunity profiling. Nat. Methods *12*, 380–381. https://doi.org/10.1038/nmeth.3364.

Borghaei, H., Paz-Ares, L., Horn, L., Spigel, D.R., Steins, M., Ready, N.E., Chow, L.Q., Vokes, E.E., Felip, E., Holgado, E., et al. (2015). Nivolumab versus docetaxel in advanced nonsquamous non-small-cell lung cancer. N. Engl. J. Med. *373*, 1627–1639. https://doi.org/10.1056/NEJMoa1507643.

Brahmer, J., Reckamp, K.L., Baas, P., Crino, L., Eberhardt, W.E., Poddubskaya, E., Antonia, S., Pluzanski, A., Vokes, E.E., Holgado, E., et al. (2015). Nivolumab versus docetaxel in advanced squamous-cell non-small-cell lung cancer. N. Engl. J. Med. *373*, 123–135. https://doi.org/10.1056/NEJMoa1504627.

Cabrita, R., Lauss, M., Sanna, A., Donia, M., Skaarup Larsen, M., Mitra, S., Johansson, I., Phung, B., Harbst, K., Vallon-Christersson, J., et al. (2020). Tertiary lymphoid structures improve immunotherapy and survival in melanoma. Nature *577*, 561–565. https://doi.org/10.1038/s41586-019-1914-8.

Chen, D.S., and Mellman, I. (2013). Oncology meets immunology: the cancer-immunity cycle. Immunity *39*, 1–10. https://doi.org/10.1016/j.immuni.2013.07.012.

Coulie, P.G., Van den Eynde, B.J., van der Bruggen, P., and Boon, T. (2014). Tumour antigens recognized by T lymphocytes: at the core of cancer immunotherapy. Nat. Rev. Cancer *14*, 135–146. https://doi.org/10.1038/nrc3670.

Crotty, S. (2019). T follicular helper cell biology: a decade of discovery and diseases. Immunity *50*, 1132–1148. https://doi.org/10.1016/j.immuni.2019.04.011.

Dammeijer, F., van Gulijk, M., Mulder, E.E., Lukkes, M., Klaase, L., van den Bosch, T., van Nimwegen, M., Lau, S.P., Latupeirissa, K., Schetters, S., et al. (2020). The PD-1/PD-L1-checkpoint restrains T cell immunity in tumor-draining lymph nodes. Cancer Cell. https://doi.org/10.1016/j.ccell.2020.09.001.

Emerson, R.O., DeWitt, W.S., Vignali, M., Gravley, J., Hu, J.K., Osborne, E.J., Desmarais, C., Klinger, M., Carlson, C.S., Hansen, J.A., et al. (2017). Immunosequencing identifies signatures of cytomegalovirus exposure history and HLA-mediated effects on the T cell repertoire. Nat. Genet. *49*, 659–665. https://doi.org/10.1038/ng.3822.

Ferris, R.L., Blumenschein, G., Fayette, J., Guigay, J., Colevas, A.D., Licitra, L., Harrington, K., Kasper, S., Vokes, E.E., Even, C., et al. (2016). Nivolumab for recurrent squamous-cell carcinoma of the head and neck. N. Engl. J. Med. *375*, 1856–1867. https://doi.org/10.1056/NEJMoa1602252.

Forde, P.M., Chaft, J.E., Smith, K.N., Anagnostou, V., Cottrell, T.R., Hellmann, M.D., Zahurak, M., Yang, S.C., Jones, D.R., Broderick, S., et al. (2018). Neoadjuvant PD-1 blockade in resectable lung cancer. N. Engl. J. Med. *378*, 1976–1986. https://doi.org/10.1056/NEJMoa1716078.

Förster, R., Braun, A., and Worbs, T. (2012). Lymph node homing of T cells and dendritic cells via afferent lymphatics. Trends Immunol. *33*, 271–280. https://doi.org/10.1016/j.it.2012.02.007.

Francis, D.M., Manspeaker, M.P., Schudel, A., Sestito, L.F., O'Melia, M.J., Kissick, H.T., Pollack, B.P., Waller, E.K., and Thomas, S.N. (2020). Blockade of immune checkpoints in lymph nodes through locoregional delivery augments cancer immunotherapy. Sci. Transl. Med. *12*. https://doi.org/10.1126/scitranslmed.aay3575.

Gros, A., Parkhurst, M.R., Tran, E., Pasetto, A., Robbins, P.F., Ilyas, S., Prickett, T.D., Gartner, J.J., Crystal, J.S., Roberts, I.M., et al. (2016). Prospective identification of neoantigen-specific lymphocytes in the peripheral blood of melanoma patients. Nat. Med. *22*, 433–438. https://doi.org/10.1038/nm.4051.

Gros, A., Robbins, P.F., Yao, X., Li, Y.F., Turcotte, S., Tran, E., Wunderlich, J.R., Mixon, A., Farid, S., Dudley, M.E., et al. (2014). PD-1 identifies the patient-specific CD8$^+$ tumor-reactive repertoire infiltrating human tumors. J. Clin. Invest. *124*, 2246–2259. https://doi.org/10.1172/JCI73639.

Hafemeister, C., and Satija, R. (2019). Normalization and variance stabilization of single-cell RNA-seq data using regularized negative binomial regression. Genome Biol. *20*, 296. https://doi.org/10.1186/s13059-019-1874-1.

Helmink, B.A., Reddy, S.M., Gao, J., Zhang, S., Basar, R., Thakur, R., Yizhak, K., Sade-Feldman, M., Blando, J., Han, G., et al. (2020). B cells and tertiary lymphoid structures promote immunotherapy response. Nature *577*, 549–555. https://doi.org/10.1038/s41586-019-1922-8.

Herbst, R.S., Soria, J.C., Kowanetz, M., Fine, G.D., Hamid, O., Gordon, M.S., Sosman, J.A., McDermott, D.F., Powderly, J.D., Gettinger, S.N., et al. (2014). Predictive correlates of response to the anti-PD-L1 antibody MPDL3280A in cancer patients. Nature *515*, 563–567. https://doi.org/10.1038/nature14011.

Hodi, F.S., O'Day, S.J., McDermott, D.F., Weber, R.W., Sosman, J.A., Haanen, J.B., Gonzalez, R., Robert, C., Schadendorf, D., Hassel, J.C., et al. (2010). Improved survival with ipilimumab in patients with metastatic melanoma. N. Engl. J. Med. *363*, 711–723. https://doi.org/10.1056/NEJMoa1003466.

Hollern, D.P., Xu, N., Thennavan, A., Glodowski, C., Garcia-Recio, S., Mott, K.R., He, X., Garay, J.P., Carey-Ewend, K., Marron, D., et al. (2019). B cells and T follicular helper cells mediate response to checkpoint inhibitors in high mutation burden mouse models of breast cancer. Cell *179*, 1191–1206.e21. https://doi.org/10.1016/j.cell.2019.10.028.

Hoof, I., Peters, B., Sidney, J., Pedersen, L.E., Sette, A., Lund, O., Buus, S., and Nielsen, M. (2009). NetMHCpan, a method for MHC class I binding prediction beyond humans. Immunogenetics *61*, 1–13. https://doi.org/10.1007/s00251-008-0341-z.

Hulpke, S., and Tampe, R. (2013). The MHC I loading complex: a multitasking machinery in adaptive immunity. Trends Biochem. Sci. *38*, 412–420. https://doi.org/10.1016/j.tibs.2013.06.003.

Inamori, K., Togashi, Y., Fukuoka, S., Akagi, K., Ogasawara, K., Irie, T., Motooka, D., Kobayashi, Y., Sugiyama, D., Kojima, M., et al. (2021). Importance of lymph node immune responses in MSI-H/dMMR colorectal cancer. JCI Insight. https://doi.org/10.1172/jci.insight.137365.

Inozume, T., Yaguchi, T., Ariyasu, R., Togashi, Y., Ohnuma, T., Honobe, A., Nishikawa, H., Kawakami, Y., and Kawamura, T. (2019). Analysis of the tumor reactivity of tumor-infiltrating lymphocytes in a metastatic melanoma lesion that lost MHC class I expression after anti-PD-1 therapy. J. Invest. Dermatol. https://doi.org/10.1016/j.jid.2019.01.007.

Jurtz, V., Paul, S., Andreatta, M., Marcatili, P., Peters, B., and Nielsen, M. (2017). NetMHCpan-4.0: improved peptide-MHC class I interaction predictions integrating eluted ligand and peptide binding affinity data. J. Immunol. *199*, 3360–3368. https://doi.org/10.4049/jimmunol.1700893.

Kamada, T., Togashi, Y., Tay, C., Ha, D., Sasaki, A., Nakamura, Y., Sato, E., Fukuoka, S., Tada, Y., Tanaka, A., et al. (2019). PD-1$^+$ regulatory T cells amplified by PD-1 blockade promote hyperprogression of cancer. Proc. Natl. Acad. Sci. U S A *116*, 9999–10008. https://doi.org/10.1073/pnas.1822001116.

Kumagai, S., Togashi, Y., Kamada, T., Sugiyama, E., Nishinakamura, H., Takeuchi, Y., Vitaly, K., Itahashi, K., Maeda, Y., Matsui, S., et al. (2020a). The PD-1 expression balance between effector and regulatory T cells predicts the clinical efficacy of PD-1 blockade therapies. Nat. Immunol. *21*, 1346–1358. https://doi.org/10.1038/s41590-020-0769-3.

Kumagai, S., Togashi, Y., Sakai, C., Kawazoe, A., Kawazu, M., Ueno, T., Sato, E., Kuwata, T., Kinoshita, T., Yamamoto, M., et al. (2020b). An oncogenic alteration creates a microenvironment that promotes tumor progression by conferring a metabolic advantage to regulatory T cells. Immunity *53*, 187–203.e8. https://doi.org/10.1016/j.immuni.2020.06.016.

Larkin, J., Hodi, F.S., and Wolchok, J.D. (2015). Combined nivolumab and ipilimumab or monotherapy in untreated melanoma. N. Engl. J. Med. *373*, 1270–1271. https://doi.org/10.1056/NEJMc1509660.

Li, B., Li, T., Pignon, J.C., Wang, B., Wang, J., Shukla, S.A., Dou, R., Chen, Q., Hodi, F.S., Choueiri, T.K., et al. (2016). Landscape of tumor-infiltrating T cell repertoire of human cancers. Nat. Genet. *48*, 725–732. https://doi.org/10.1038/ng.3581.

Li, H., van der Leun, A.M., Yofe, I., Lubling, Y., Gelbard-Solodkin, D., van Akkooi, A.C.J., van den Braber, M., Rozeman, E.A., Haanen, J.B.A.G., Blank, C.U., et al. (2019). Dysfunctional CD8 T cells form a proliferative, dynamically regulated compartment within human melanoma. Cell *176*, 775–789.e18. https://doi.org/10.1016/j.cell.2018.11.043.

Lim, B., Lin, Y., and Navin, N. (2020). Advancing cancer research and medicine with single-cell genomics. Cancer Cell *37*, 456–470. https://doi.org/10.1016/j.ccell.2020.03.008.

Niogret, J., Berger, H., Rebe, C., Mary, R., Ballot, E., Truntzer, C., Thibaudin, M., Derangère, V., Hibos, C., Hampe, L., et al. (2021). Follicular helper-T cells restore CD8$^+$-dependent antitumor immunity and anti-PD-L1/PD-1 efficacy. J. Immunother. Cancer *9*. https://doi.org/10.1136/jitc-2020-002157.

Oliveira, G., Stromhaug, K., Klaeger, S., Kula, T., Frederick, D.T., Le, P.M., Forman, J., Huang, T., Li, S., Zhang, W., et al. (2021). Phenotype, specificity and avidity of antitumour CD8+ T cells in melanoma. Nature. https://doi.org/10.1038/s41586-021-03704-y.

Papalexi, E., and Satija, R. (2018). Single-cell RNA sequencing to explore immune cell heterogeneity. Nat. Rev. Immunol. *18*, 35–45. https://doi.org/10.1038/nri.2017.76.

Petitprez, F., de Reyniès, A., Keung, E.Z., Chen, T.W., Sun, C.M., Calderaro, J., Jeng, Y.M., Hsiao, L.P., Lacroix, L., Bougoüin, A., et al. (2020). B cells are associated with survival and immunotherapy response in sarcoma. Nature *577*, 556–560. https://doi.org/10.1038/s41586-019-1906-8.

Popic, V., Salari, R., Hajirasouliha, I., Kashef-Haghighi, D., West, R.B., and Batzoglou, S. (2015). Fast and scalable inference of multi-sample cancer lineages. Genome Biol. *16*, 91. https://doi.org/10.1186/s13059-015-0647-8.

Rizvi, N.A., Hellmann, M.D., Snyder, A., Kvistborg, P., Makarov, V., Havel, J.J., Lee, W., Yuan, J., Wong, P., Ho, T.S., et al. (2015). Cancer immunology. Mutational landscape determines sensitivity to PD-1 blockade in non-small cell lung cancer. Science *348*, 124–128. https://doi.org/10.1126/science.aaa1348.

Roth, A., Khattra, J., Yap, D., Wan, A., Laks, E., Biele, J., Ha, G., Aparicio, S., Bouchard-Côté, A., and Shah, S.P. (2014). PyClone: statistical inference of clonal population structure in cancer. Nat. Methods *11*, 396–398. https://doi.org/10.1038/nmeth.2883.

Sade-Feldman, M., Yizhak, K., Bjorgaard, S.L., Ray, J.P., de Boer, C.G., Jenkins, R.W., Lieb, D.J., Chen, J.H., Frederick, D.T., Barzily-Rokni, M., et al. (2018). Defining T cell states associated with response to checkpoint immunotherapy in melanoma. Cell *175*, 998–1013.e1020. https://doi.org/10.1016/j.cell.2018.10.038.

Scheper, W., Kelderman, S., Fanchi, L.F., Linnemann, C., Bendle, G., de Rooij, M.A.J., Hirt, C., Mezzadra, R., Slagter, M., Dijkstra, K., et al. (2019). Low and variable tumor reactivity of the intratumoral TCR repertoire in human cancers. Nat. Med. *25*, 89–94. https://doi.org/10.1038/s41591-018-0266-5.

Schreiber, R.D., Old, L.J., and Smyth, M.J. (2011). Cancer immunoediting: integrating immunity's roles in cancer suppression and promotion. Science *331*, 1565–1570. https://doi.org/10.1126/science.1203486.

Shen, R., and Seshan, V.E. (2016). FACETS: allele-specific copy number and clonal heterogeneity analysis tool for high-throughput DNA sequencing. Nucleic Acids Res. *44*, e131. https://doi.org/10.1093/nar/gkw520.

Simoni, Y., Becht, E., Fehlings, M., Loh, C.Y., Koo, S.L., Teng, K.W.W., Yeong, J.P.S., Nahar, R., Zhang, T., Kared, H., et al. (2018). Bystander CD8$^+$ T cells are abundant and phenotypically distinct in human tumour infiltrates. Nature *557*, 575–579. https://doi.org/10.1038/s41586-018-0130-2.

Smith, M.A., Nielsen, C.B., Chan, F.C., McPherson, A., Roth, A., Farahani, H., Machev, D., Steif, A., and Shah, S.P. (2017). E-scape: interactive visualization of single-cell phylogenetics and cancer evolution. Nat. Methods *14*, 549–550. https://doi.org/10.1038/nmeth.4303.

Stoeckius, M., Hafemeister, C., Stephenson, W., Houck-Loomis, B., Chattopadhyay, P.K., Swerdlow, H., Satija, R., and Smibert, P. (2017). Simultaneous epitope and transcriptome measurement in single cells. Nat. Methods *14*, 865–868. https://doi.org/10.1038/nmeth.4380.

Stuart, T., and Satija, R. (2019). Integrative single-cell analysis. Nat. Rev. Genet. https://doi.org/10.1038/s41576-019-0093-7.

Tirosh, I., Izar, B., Prakadan, S.M., Wadsworth, M.H., Treacy, D., Trombetta, J.J., Rotem, A., Rodman, C., Lian, C., Murphy, G., et al. (2016). Dissecting the multicellular ecosystem of metastatic melanoma by single-cell RNA-seq. Science *352*, 189–196. https://doi.org/10.1126/science.aad0501.

Togashi, Y., Shitara, K., and Nishikawa, H. (2019). Regulatory T cells in cancer immunosuppression—implications for anticancer therapy. Nat. Rev. Clin. Oncol. *16*, 356–371. https://doi.org/10.1038/s41571-019-0175-7.

Topalian, S.L., Drake, C.G., and Pardoll, D.M. (2015). Immune checkpoint blockade: a common denominator approach to cancer therapy. Cancer Cell *27*, 450–461. https://doi.org/10.1016/j.ccell.2015.03.001.

Tumeh, P.C., Harview, C.L., Yearley, J.H., Shintaku, I.P., Taylor, E.J., Robert, L., Chmielowski, B., Spasic, M., Henry, G., Ciobanu, V., et al. (2014). PD-1

blockade induces responses by inhibiting adaptive immune resistance. Nature *515*, 568–571. https://doi.org/10.1038/nature13954.

Wherry, E.J. (2011). T cell exhaustion. Nat. Immunol. *12*, 492–499.

Wherry, E.J., and Kurachi, M. (2015). Molecular and cellular insights into T cell exhaustion. Nat. Rev. Immunol. *15*, 486–499. https://doi.org/10.1038/nri3862.

Wu, T.D., Madireddi, S., de Almeida, P.E., Banchereau, R., Chen, Y.J., Chitre, A.S., Chiang, E.Y., Iftikhar, H., O'Gorman, W.E., Au-Yeung, A., et al. (2020). Peripheral T cell expansion predicts tumour infiltration and clinical response. Nature *579*, 274–278. https://doi.org/10.1038/s41586-020-2056-8.

Yost, K.E., Satpathy, A.T., Wells, D.K., Qi, Y., Wang, C., Kageyama, R., McNamara, K.L., Granja, J.M., Sarin, K.Y., Brown, R.A., et al. (2019). Clonal replacement of tumor-specific T cells following PD-1 blockade. Nat. Med. https://doi.org/10.1038/s41591-019-0522-3.

Zou, W., Wolchok, J.D., and Chen, L. (2016). PD-L1 (B7-H1) and PD-1 pathway blockade for cancer therapy: mechanisms, response biomarkers, and combinations. Sci. Transl. Med. *8*, 328rv324. https://doi.org/10.1126/scitranslmed.aad7118.

STAR★METHODS

KEY RESOURCES TABLE

REAGENT or RESOURCE	SOURCE	IDENTIFIER
Antibodies		
Anti-human CD3-Alexa Fluor 700 (UCHT1)	BD Biosciences	Cat# 557943; RRID:AB_396952
Anti-human CD8a-PE-Cy7 (RPA-T8)	Biolegend	Cat# 301012; RRID:AB_314130
Anti-human CD137-APC (4B4-1)	BD Biosciences	Cat# 550890; RRID:AB_398477
PE anti-human CD69 Antibody	Biolegend	Cat# 310905; RRID:AB_314840
Anti-human TCR Vβ5.2-FITC (36213)	Beckman Coulter	Cat# IM1482; RRID:AB_130872
Anti-human TCR Vβ2-FITC (MPB2D5)	Beckman Coulter	Cat# IM2407; RRID:AB_131047
Anti-human TCR Vβ14-FITC (CAS1.1.3)	Beckman Coulter	Cat# IM1558; RRID:AB_131024
Anti-human TCRVβ8-FITC (56C5.2)	Beckman Coulter	Cat# IM1233; RRID:AB_130922
Anti-human TCR Vβ3-FITC (CH92)	Beckman Coulter	Cat# IM2372; RRID:AB_131046
Anti-human TCR Vβ13.1-FITC (IMMU 222)	Beckman Coulter	Cat# IM1554; RRID:AB_130874
Anti-human TCR Vβ21.3-FITC (IG125)	Beckman Coulter	Cat# IM1483; RRID:AB_131021
Anti-human TCR Vβ4-FITC (WJF24)	Beckman Coulter	Cat# B07084
Anti-human TCRVβ1-FITC (BL37.2)	Beckman Coulter	Cat# IM2406; RRID:AB_130880
Anti-human TCR Vβ17-FITC (E17.5F3.15.13)	Beckman Coulter	Cat# IM1234; RRID:AB_131007
Anti-human TCR Vβ12-FITC (VER2.32.1)	Beckman Coulter	Cat# IM1587; RRID:AB_131028
Anti-human IFN-g-BV421 (B27)	BD Biosciences	Cat# 562988; RRID:AB_2737934
Anti-mouse CD3-V500 (500A2)	BD Biosciences	Cat# 560771; RRID:AB_1937314
Anti-mouse CD4-PE-Cy7 (RM4-5)	BD Biosciences	Cat# 552775; RRID:AB_394461
Anti-mouse CD8a-PerCP-Cy5.5 (53-6.7)	BD Biosciences	Cat# 551162; RRID:AB_394081
Anti-mouse CD279 (PD-1)-BV421 (29F.1A12)	Biolegend	Cat# 135217; RRID:AB_10900085
Anti-human CD8a (EP1150Y)	Abcam	Cat# ab93278; RRID:AB_10563532
Purified anti-human CD3 (OKT3)	Thermo Fisher Scientific	Cat# 16-0037-81; RRID:AB_468854
Anti-mouse PD-1 (RMP1-14)	Biolegend	Cat# 114111; RRID:AB_2566089
Purified Rat IgG2a κ isotype control (RTK2758)	Biolegend	Cat# 400502
Fc Receptor Binding Inhibitor Functional Grade Polyclonal Antibody	Thermo Fisher Scientific	Cat# 16-9161-73; RRID:AB_469272
Biological samples		
Healthy donor PBMC	CTL	N/A
Chemicals, peptides, and recombinant proteins		
Fetal Bovine Serum	Cytiva	Cat# SH30396
RPMI 1640 Medium	Thermo Fisher Scientific	Cat# 11875093
Collagenase type IV	Sigma-Aldrich	Cat# C4-28-100MG
Hyaluronidase type V	Sigma-Aldrich	Cat# H6254-500MG
Deoxyribonuclease I type IV	Sigma-Aldrich	Cat# D5025-15KU
Penicillin-streptomycin	Thermo Fisher Scientific	Cat# 14150122
Amphotricin B	Thermo Fisher Scientific	Cat# 15290018
rhIL-2	PeproTech	Cat# 200-02
CCDC121_P134L (AEGPRRLLPLYHSLINNFV)	GL Biochem	N/A
DYX1C1_N305S (KGNKLFATESYLAAINAYN)	GL Biochem	N/A
SOX5_D286H (PLMIPVFPPHQRTLAAAAQ)	GL Biochem	N/A
TP53_C238K (TTIHYNYMCKNSSCMGGMN)	GL Biochem	N/A
ATHL1_H37Y (NAYLGTRVFYDTLHVSGVY)	GL Biochem	N/A
TDG_G154R (AAYKGHHYPRPGNHFWKCL)	GL Biochem	N/A

(*Continued on next page*)

Continued

REAGENT or RESOURCE	SOURCE	IDENTIFIER
CCDC121 (AEGPRRLLPPYHSLINNFV)	GL Biochem	N/A
DYX1C1 (KGNKLFATENYLAAINAYN)	GL Biochem	N/A
SOX5 (PLMIPVFPPDQRTLAAAAQ)	GL Biochem	N/A
TP53 (TTIHYNYMCNSSCMGGMN)	GL Biochem	N/A
ATHL1 (NAYLGTRVFHDTLHVSGVY)	GL Biochem	N/A
TDG (AAYKGHHYPGPGNHFWKCL)	GL Biochem	N/A
MART-1_1 (ELAGIGILTV)	GL Biochem	N/A
MART-1_2 (ALMDKSLHV)	GL Biochem	N/A
MART-1_3 (GILTVILGV)	GL Biochem	N/A
gp100_1 (YLEPGPVTA)	GL Biochem	N/A
gp100_2 (AVIGALLAV)	GL Biochem	N/A
gp100_3 (KTWGQYWQV)	GL Biochem	N/A
gp100_4 (SQVWGGQPV)	GL Biochem	N/A
gp100_5 (MLGTHTMEV)	GL Biochem	N/A
gp100_6 (AQVTTTEWV)	GL Biochem	N/A
7-AAD	Thermo Fisher Scientific	Cat# A1310
Calcein-AM	Thermo Fisher Scientific	Cat# C1430
FTY720	sigma	Cat# SML0700
Critical commercial assays		
Foxp3/Transcription Factor Staining Buffer Set	Thermo Fisher Scientific	Cat# 00-5523-00
Fixation/Permeabilization Solution Kit with BD GolgiStop	BD Biosciences	Cat# 554724
Target Retrieval Solution	Dako	Cat# K2367
LSAB2 Kit	Dako	Cat# K0675
AEC Substrate Chromogen Ready-to-Use	Dako	Cat# K3464
PCR Mycoplasma Detection Kit	TaKaRa	Cat# CY232
Lipofectamine 3000	Thermo Fisher Scientific	Cat# L3000008
RetroNectin	TaKaRa	Cat# T100B
IFN gamma Human Uncoated ELISA Kit with Plates	Thermo Fisher Scientific	Cat# 88-7316-22
QUANTI-Luc	InvivoGen	Cat# rep-qlc2
Bright-Glo™ Luciferase Assay System	Promega	Cat# E2610
SMARTer RACE 5'/3' Kit	TaKaRa	Cat# 634858
SMARTer Mouse TCRa/b Profiling Kit	TaKaRa	Cat# 634402
Chromium Next GEM Chip K Single Cell Kit	10× Genomics	Cat# 1000287
Chromium Next GEM Single Cell 5' Kit	10× Genomics	Cat# 1000265
Chromium Single Cell Human TCR Amplification Kit	10× Genomics	Cat# 1000252
Dual Index Kit TT set A	10× Genomics	Cat# 1000215
Library Construction Kit	10× Genomics	Cat# 1000190
Dynabeads MyOne SILANE	Thermo Fisher Scientific	Cat# 37002D
SPRIselect beads	Beckman Coulter	Cat# B23318
QIAamp DNA Mini Kit	QIAGEN	Cat# 51304
RNeasy Mini Kit	QIAGEN	Cat# 74104
NEBNext Ultra DNA Library Prep Kit for Illumina	New England BioLabs	Cat# E7370S
SureSelect Human All Exon Kit V6	Agilent Technologies	Cat# 5190-8869
NEBNext Ultra RNA Library Prep Kit for Illumina	New England BioLabs	Cat# E7530S
Deposited data		
Single-cell sequencing for melanoma samples	This paper	DDBJ: JGAS000285
Single-cell sequencing for lung cancer and head and neck cancer samples	This paper	DDBJ: JGAS000480

(*Continued on next page*)

Continued

REAGENT or RESOURCE	SOURCE	IDENTIFIER
WES and RNA-seq	This paper	DDBJ: JGAS000285
Mouse TCR sequencing	This paper	DDBJ: DRA013159
Publicly available TCR datasets of healthy donors	Emerson et al. (2017)	https://clients.adaptivebiotech.com/pub/Emerson-2017-NatGen
Publicly available TCR datasets of TCGA	Li et al. (2016)	https://clients.adaptivebiotech.com/pub/Liu-2016-NatGenetics
Previously published scRNA-seq, scTCR-seq, and bulk TCR-seq datasets	Yost et al. (2019)	GEO: GSE123814
Experimental models: Cell lines		
B2M-transduced MEL01	N/A	N/A
MEL02-1	N/A	N/A
MEL02-2	N/A	N/A
MEL03	N/A	N/A
E.G7	ATCC	Cat# CRL-2113
B16F10	ATCC	Cat# CRL-6475
MC-38	Kerafast	Cat# ENH204
Jurkat, Clone E6-1	ATCC	Cat# TIB-152
Experimental models: Organisms/strains		
C57BL/6	CLEA	N/A
Recombinant DNA		
pMSCV	VectorBuilder	N/A
pVSV-G	TaKaRa	Cat# 631530
pGL4.30 [luc2P/NFAT-RE/Hygro] Luciferase Reporter Vectors	Promega	Cat# 9PIE848
Software and algorithms		
FlowJo 10.0.8	BD Biosciences	N/A
GraphPad Prism 7	GraphPad Software Inc.	N/A
R version 4.0.2	R Foundation for Statistical Computing	N/A
Seurat versions 3.2, 4.0beta	https://satijalab.org/seurat/	N/A
MiXCR version 3.0.13	Bolotin, D., Poslavsky, S., Mitrophanov, I. et al. MiXCR: software for comprehensive adaptive immunity profiling. Nat Methods 12, 380–381 (2015). https://doi.org/10.1038/nmeth.3364	N/A
Python version 3.8.3	Python Software Foundation	N/A
Seaborn version 0.11.0	https://seaborn.pydata.org/index.html	N/A

RESOURCE AVAILABILITY

Lead contact

Further information and requests for resources and reagents should be directed to and will be fulfilled by the lead contact, Yosuke Togashi (ytogashi1584@gmail.com).

Materials availability

Plasmids and cell lines generated in this study are available from the lead contact, but we may require a completed materials transfer agreement.

Data and code availability

- scRNA-seq, scTCR-seq, TCR-seq, RNA-seq and Whole-exome sequencing data have been deposited at DDBJ and are publicly available as of the date of publication. Accession numbers are listed in the key resources table. Original plate

reader measurements and flow cytometry measurements ported in this paper will be shared by the lead contact upon request.

- This paper does not report original code.
- Any additional information required to reanalyze the data reported in this paper is available from the lead contact upon request.

EXPERIMENTAL MODEL AND SUBJECT DETAILS

Patients and samples

Three patients with melanoma who underwent surgical resection and received PD-1 blockade therapy at Yamanashi University Hospital from 2017 to 2019 and 3 patients with other cancers (lung adenocarcinoma and head-and-neck squamous cell carcinoma) who underwent surgical resection and did not receive PD-1 blockade therapy at Chiba Cancer Center in 2020 were enrolled in this study (Table S1). To collect nonmetastatic TDLNs, the dissected TDLNs were halved at the greatest circumference (maximum surface) and subjected to pathological examination; for those samples diagnosed as non-metastatic LNs, the remaining portions were subjected to further analyses. The patients' clinical information was obtained from their medical records. The protocol for this study was approved by the appropriate institutional review board and ethics committees at the Yamanashi University Hospital and Chiba Cancer Center. This study was conducted in accordance with the Declaration of Helsinki.

Patient tumor and LN specimens were processed as described previously (Inozume et al., 2019). Briefly, surgically resected samples were enzymatically digested with 0.1% collagenase type IV, 0.01% hyaluronidase type V, and 30 U/mL deoxyribonuclease I type IV (Sigma-Aldrich, St. Louis, MO) in RPMI 1640 (Thermo Fisher Science, Waltham, MA) at room temperature. After filtration and separation by density gradient, the digested tumor cells were cryopreserved until use.

Cell lines

To establish tumor cell lines, 1×10^7 digested tumor cells were cultured in RPMI 1640 containing 10% fetal bovine serum (FBS; Cytiva, Tokyo, Japan), penicillin-streptomycin, and amphotericin B (Thermo Fisher Science). Tumor cells were passaged at approximately 80%–90% confluence and used when free of fibroblasts and proliferated beyond the 10th passage. The MEL01 cell line was generated from a previously reported melanoma patient who acquired resistance after an initial response to PD-1 blockade therapy (Inozume et al., 2019). This cell line exhibited B2M gene loss and no MHC class I expression (Inozume et al., 2019). Both MEL02 and MEL03 cell lines were generated from melanoma superresponders to PD-1 blockade therapy. The MEL02-1 cell line was obtained before initiation of PD-1 blockade therapy, and the MEL02-2 cell line was obtained after PD-1 blockade therapy in a site-matched manner (Table S1 and Figure S1).

E.G7 (mouse lymphoma), B16F10 (mouse melanoma), and Jurkat cell lines were purchased from ATCC (Manassas, VA; ATCC Cat#CRL-2113, RRID: CVCL_3505, ATCC Cat#CRL-6475, RRID: CVCL_0159, and ATCC Cat#TIB-152, RRID: CVCL_0367, respectively). The MC-38 cell line (mouse colon cancer) was purchased from Kerafast (Boston, MA; Cat# ENH204, RRID: CVCL_B288). E.G7, B16F10, and Jurkat cell lines were maintained in RPMI 1640 medium supplemented with 10% FBS, and the MC-38 cell line was maintained in DMEM (Thermo Fisher Science) supplemented with 10% FBS. All tumor cells were used after confirming that they were *Mycoplasma* (−) by the PCR Mycoplasma Detection Kit (TaKaRa, Shiga, Japan) according to the manufacturer's instructions.

In vivo animal models

Female C57BL/6J mice (6-8 weeks old) were purchased from CLEA Japan (Tokyo, Japan). Cells (1×10^6) were injected subcutaneously, and the tumor volume was monitored twice a week. The means of the long and short tumor diameters were used to generate tumor growth curves. Mice were grouped when the tumor volume reached approximately 100 mm^3 (day 0), and anti-PD-1 mAb (200 μg/mouse) or control mAb was administered intraperitoneally three times every 3 days thereafter with or without FTY720. FTY720 (25 μg/mouse on day 1 and 5 μg/mouse on day 2∼) was administered intraperitoneally every day. Tumors were harvested at baseline (approximately 100 mm^3) and at 9 days after initiation of treatment to collect TILs for evaluation. Rat anti-mouse PD-1 mAb (RMP1-14) and control rat IgG2a mAb (RTK2758) were purchased from BioLegend (San Diego, CA), and FTY720 was purchased from Sigma-Aldrich (St. Louis, MO). We confirmed that the PD-1 clone RMP1-14 was not competitive with clone 29F.1A12, which we used to analyze PD-1 expression by flow cytometry (Figure S7B). *In vivo* experiments were performed at least twice. All mice were maintained under specific pathogen-free conditions in the animal facility of the Institute of Biophysics. Mouse experiments were approved by the Animal Committee for Animal Experimentation of the Chiba Cancer Center. All experiments met the U.S. Public Health Service Policy on the Humane Care and Use of Laboratory Animals.

METHOD DETAILS

Immunohistochemistry

Sections of formalin-fixed, paraffin-embedded tissue (5 μm) were dried and subsequently dewaxed and rehydrated. Endogenous peroxidase activity was blocked by incubation with 0.3% hydrogen peroxide in methanol. After antigen retrieval by boiling for

10 min in 10 mmol/L citrate buffer (pH 9.0), the tissue sections were incubated overnight with anti-CD8 mAb (Abcam, Cambridge, UK; clone EP1150Y). Then, immunoreactivity was detected using the LSAB2 Kit and AEC Substrate Chromogen (Dako, Copenhagen, Denmark), and counterstaining was performed using Mayer's hematoxylin.

scRNA-seq and scTCR-seq

The scRNA-seq and scTCR-seq libraries were prepared using the 10× Single Cell Immune Profiling Solution Kit according to the manufacturer's instructions. In brief, $CD3^+$ T cells sorted by FACSAria (BD Biosciences, Franklin Lakes, NJ) were washed and resuspended in PBS with 0.5% FBS. Cells were captured in droplets at a targeted cell recovery of <10,000 cells. Following reverse transcription and cell barcoding in droplets, the emulsions were broken, and the cDNA was purified using Dynabeads MyOne SILANE (Thermo Fisher Scientific), followed by PCR amplification. Amplified cDNA was then used for both 5′ gene expression library construction and TCR enrichment. For gene expression library construction, 2.4–50 ng of amplified cDNA was fragmented, end-repaired, double-sided size-selected with SPRIselect beads (Beckman Coulter, Brea, CA), PCR-amplified with sample indexing primers, and again double-sided size-selected with SPRIselect beads. For TCR library construction, TCR transcripts were enriched from 2 μL of amplified cDNA by PCR. Following TCR enrichment, 5–50 ng of enriched PCR product was fragmented and end-repaired, size-selected with SPRIselect beads, PCR-amplified with sample-indexing primers, and again size-selected with SPRIselect beads. The scRNA libraries were sequenced on a HiSeq 3000 (Illumina, San Diego, CA) or DNBSEQ-G400 (MGI Tech, Shenzhen, China) instrument to a minimum sequencing depth of 25,000 reads per cell. The single-cell TCR libraries were sequenced on a HiSeq 3000 or DNBSEQ-G400 instrument to a minimum sequencing depth of 5,000 reads per cell. Sequencing read lengths were adjusted for each library type according to the manufacturer's instructions and reagent version.

Data analysis for single cell sequencing

Single-cell library reads were processed using CellRanger software (version 4.0.0). UMI count matrices were loaded using the Seurat R package (Hafemeister and Satija, 2019), and cells with a mitochondrial content above 10% and cells with less than 200 or more than 4000 genes detected were considered outliers (dying cells, empty droplets, doublets, respectively) and filtered out. The Seurat NormalizeData function was used for normalization, and data were integrated using the IntegrateData function. Finally, dimensionality reduction was performed by running PCA and then computing UMAP embeddings using the first 25 components of the PCA for visualization and clustering. Clusters were manually annotated based on the expression of known flow cytometry and single-cell marker genes, including*CD3D*, *CD3E*, and *CD2* (T cells), *CD8A*, *CD4*, and *CCR7* (naive $CD4^+$/$CD8^+$ T cells), *FOXP3* (regulatory T cells), GZMA (combined with CD4 detection and lack of CD8, cytotoxic $CD4^+$ T cells), *CD200* (follicular helper T cells), EOMES (memory $CD8^+$ T cells), *PDCD1* and *HAVCR2* (exhausted $CD8^+$ T cells). Clusters were also confirmed on the basis of differentially expressed marker genes for each cluster and comparison to known cell-type-specific marker genes.

TCR reads were aligned to the GRCh38 reference genome, and consensus TCR annotation was performed using cellranger vdj (10× Genomics, version 4.0.0). TCR libraries were sequenced to a minimum depth of 5,000 reads per cell. TCR annotation was performed using the 10× cellranger vdj pipeline according to the manufacturer's instructions. Because most of the matching to public bulk TCR datasets is performed at the TCRβ level, cells without a reconstructed TCRα clonotype were kept, while cells lacking a TCRβ clonotype were not retained for downstream analysis. For cells with two or more clonotypes for a given chain, the clonotype with the highest number of UMIs was used, and cells were labeled as ambiguous if the second clonotype had more than half the number of UMIs of the top clonotype.

In vitro expansion of TILs

TILs were expanded as described previously (Inozume et al., 2019). In brief, melanoma tumor digests were inoculated into RPMI 1640 supplemented with 10% human AB serum, antibiotics, and recombinant human interleukin-2 (rhIL-2: 6,000 IU/mL, PeproTech, Cranbury, NJ) in a humidified 37°C incubator with 5% CO_2. After 5 days, half of the media was aspirated from the wells and replaced with fresh complete medium and rhIL-2; this procedure was repeated every 2-3 days thereafter as needed.

Enrichment of tumor-specific T cell clones, cloning, and identification of TCR clonotypes

The procedure is summarized in Figure S3A. Briefly, $CD8^+$ T cells (1×10^6 cells per well) purified from expanded TILs were cocultured with a 100-Gy-irradiated autologous tumor cell line (1×10^6 cells per well). After 12 h, the cells sorted using anti-human CD137-APC mAb (4B4-1, BD Biosciences) were expanded with irradiated PBMCs from allogeneic donors and anti-CD3 mAb (30 ng/mL OKT-3, Thermo Fisher Scientific). rhIL-2 (300 IU/mL) was added on the next day, and the medium was replenished on day 5. Thereafter, T cell clones were established by limiting dilution as previously described (Inozume et al., 2019). The clonality of the expanded T cells was verified by TCRα and TCRβ chain V region (TRAV and TRBV, respectively) analysis based on the 5′ RACE method using the SMARTer RACE 5′/3′ Kit (TaKaRa) as previously described (Inozume et al., 2019).

Constructs, virus production, and transfection

Each TCRα- and β-transduced pMSCV vector created by VectorBuilder (Chicago, IL) and pVSV-G vector (TaKaRa) were transfected into packaging cells using Lipofectamine 3000 Reagent (Thermo Fisher Scientific). After 48 hours, the supernatant was concentrated and transfected into the NFAT-Jurkat cell line or $CD8^+$ T cells from healthy donors using RetroNectin Reagent (TaKaRa).

IFN-γ release assay

Cultured autologous tumor cell lines (10^5 cells/well) were used as stimulator cells. Clonally enriched $CD8^+$ T cells or TCR-transduced $CD8^+$ T cells at 10^4–10^5 cells/well were added to the tumor cells and incubated for 48 hours. Supernatants were assayed by ELISA for IFN-γ (Thermo Fisher Science), and IFN-γ production by T cells was analyzed with flow cytometry. *In vitro* experiments were performed in triplicate.

Killing assay

Killing assays were performed using calcein-AM (Thermo Fisher Science). Briefly, calcein-AM-labeled tumor cells (target cells; T) were cocultured with clonally enriched $CD8^+$ T cells (effector cells; E) at the indicated E/T ratios and then centrifuged to ensure contact between the cell populations. Fluorescence was measured at 3 hours of incubation. *In vitro* experiments were performed in triplicate.

Luciferase reporter assay for tumor-specificity

A stable pGL4.30 [luc2P/NFAT-RE/Hygro] vector (Promega, Madison, WI)-transduced Jurkat cell line was established (NFAT-Jurkat cell line). Each TCR-transduced NFAT-Jurkat cell line, which was confirmed using anti-TCR mAb, was cocultured with autologous tumor cell lines. At 24 hours after coculture, luciferase activity was analyzed using the Bright-Glo Luciferase Assay System (Promega) according to the manufacturer's instructions. We compared the data with those from experiments without autologous tumor cell lines for statistical analyses, and the fold change in each NFAT-Jurkat cell line without tumor cell lines was calculated. Control clonotypes #0 and #3-0 were selected from minor clones in the TME that were frequently found in MHC-matched Adaptive Biotechnologies public PBL datasets (Emerson et al., 2017). *In vitro* experiments were performed in triplicate.

Whole-exome sequencing

Genomic DNA was isolated from each cell line using a QIAamp DNA Mini Kit (QIAGEN, Hulsterweg, Netherlands) and enriched for exonic fragments using the SureSelect Human All Exon Kit v6 (Agilent Technologies, Santa Clara, CA). Massively parallel sequencing of isolated fragments was performed with a HiSeq3000 instrument (Illumina, San Diego, CA) using the paired-end option. Whole exome sequencing reads which were masked nucleotides with less than quality value 20 were independently aligned to the human reference genome (hg38) using BWA (http://bio-bwa.sourceforge.net/) and Bowtie2 (http://bowtie-bio.sourceforge.net/bowtie2/index.shtml). Both somatic synonymous and non-synonymous mutations were called using our in-house caller and two publicly available mutation callers: Genome Analysis Toolkit (https://gatk.broadinstitute.org/hc/en-us) MuTect2 and VarScan2 (http://varscan.sourceforge.net/). Mutations were discarded if any of the following criteria were met: the total read number was <20, the variant allele frequency in tumor samples was <0.05, the mutant read number in the germline control samples was >2, the mutation occurred in only one strand of the genome, or the variant was present in normal human genomes in either the 1000 Genomes Project dataset (https://www.internationalgenome.org/) or our in-house database. Gene mutations were annotated by SnpEff (https://pcingola.github.io/SnpEff/). Copy number status was analyzed using our in-house pipeline, which determines the logR ratio (LRR) as follows: (1) SNP positions in the 1000 Genomes Project database that were in a homozygous state (VAF ≤ 0.05 or ≥ 0.95) or a heterozygous state (VAF 0.4–0.6) in the genomes of respective normal samples were selected, (2) normal and tumor read depths at the selected position were adjusted based on the G+C percentage of a 100 bp window flanking the position, (3) the LRR was calculated as $\log_2 \frac{t_i}{n_i}$, where n_i and t_i are normal and tumor-adjusted depths at position i, and (4) each representative LRR was determined as the median of a moving window (1 Mb) centered at position i.

Transcriptome sequencing and expression analysis

Total RNA was extracted from each cell line with an RNeasy Mini Kit (QIAGEN). RNA integrity was evaluated using a TapeStation (Agilent Technologies). Sequencing libraries for RNA-seq were prepared with a NEBNext Ultra RNA Library Prep Kit (New England BioLabs, Ipswich, MA) in which cDNA was prepared from polyA-selected RNA. Prepared RNA-seq libraries underwent next-generation sequencing from both ends (paired-end reads). The expression level of each gene was calculated using DESeq2 (http://bioconductor.org/packages/release/bioc/html/DESeq2.html) with VST transformation.

Clonal analysis in tumor cells

Copy number alterations were detected with FACETS (Shen and Seshan, 2016). The cellular prevalence of clones carrying individual nonsynonymous mutations was determined with PyClone (Roth et al., 2014). The determined cellular prevalence was used as input, and the phylogenetic relationships of the clones were inferred with LICHeE (Popic et al., 2015). The results were visualized with the Timescape package in R (Smith et al., 2017).

Analyses of public datasets

We merged our TIL data with two publicly available TCR datasets. We first used Adaptive Biotechnologies' publicly available healthy donor PBL datasets (Emerson et al., 2017). From these datasets, a subset of patients sharing at least one HLA-A or HLA-B allele with our patients was used, and the comparison was performed at the TCRβ (TRBV gene, CDR3β, and TRBJ gene) level. We next used a previously published dataset of CDR3s extracted from TCGA RNA-seq data (Li et al., 2016) and performed comparisons at the CDR3

level without MHC matching. In addition, we reanalyzed previously published scRNA-seq, scTCR-seq, and bulk TCR-seq datasets (Yost et al., 2019).

Antigen prediction

The NetMHCpan algorithm version 4.0 was used to predict the possible neoantigens from the whole-exome and transcriptome sequencing data (Hoof et al., 2009; Jurtz et al., 2017). The residues surrounding the amino acids resulting from nonsynonymous mutations expressed from transcriptome data were scanned to identify candidate 9-mer peptides that were predicted to bind to the MHC class I alleles of the cells. In addition, the amino acid sequences of Melan A/MART-1 and gp100 were also scanned similarly. Strong binding peptides with %Rank $\leq$0.5 were used for assays (Table S6).

Peptide assay

TCR-transduced NFAT-Jurkat cell lines that responded to autologous tumor cell lines were cocultured with irradiated autologous tumor cells after each peptide pulse. We used predicted antigen peptides derived from somatic mutations, wild-type peptides of these antigens, representative well-known Melan A/MART-1 and gp100 (CT antigens) peptides binding to HLA-A *02:01 (26-35, ELAGIGILTV; 280-288, YLEPGPVTA respectively), and predicted Melan A/MART-1 and gp100 peptides binding to HLA-A *02:06 (Table S6). Luciferase activity was analyzed after 24 hours of coculture. We compared wild-type peptide-pulse data (predicted mutated antigens) or nonpulse data (CT antigens) for statistical analyses, and the fold change in each NFAT-Jurkat cell line that received a wild-type-peptide pulse (predicted mutated antigens) or did not receive a peptide pulse (CT antigens) was calculated. *In vitro* experiments were performed in triplicate.

Mouse TCR sequencing and data analyses

After PD-1^{+}CD8^{+} T cells were sorted using FACSMelody (BD Biosciences), the extracted RNA was subjected to TCR sequencing with the SMARTer Mouse TCRa/b Profiling Kit (TaKaRa) according to the manufacturer's instructions. TCR libraries were sequenced using the Illumina MiSeq platform (Illumina) and a 2 × 300 bp paired-end kit. Reads were assembled and aligned to mouse VDJ reference genes using MiXCR software with the default parameters (Bolotin et al., 2015).

Flow cytometry analyses

Flow cytometry assays were performed as described (Kumagai et al., 2020b). Briefly, cells were washed with PBS containing 2% FBS and subjected to staining with surface antibodies. Intracellular staining was performed with specific antibodies and the FOXP3/Transcription Factor Staining Buffer Set (Thermo Fisher Scientific) according to the manufacturer's instructions. For intracellular cytokine staining, GolgiStop reagent (BD Biosciences) was added for the last 4 hours of culture. Samples were assessed with a BD FACSVerse instrument (BD Biosciences) and FlowJo software (BD Biosciences). The staining antibodies were diluted following the manufacturer's instructions.

QUANTIFICATION AND STATISTICAL ANALYSIS

GraphPad Prism 7 (GraphPad Software, San Diego, CA) and R version 4.0.2 (R Foundation for Statistical Computing, Vienna, Austria) were used for the statistical analyses. Differential gene expression analysis on single-cell datasets was performed through the FindMarkers function of the Seurat R package using the Wilcoxon rank sum test. The categorical variables were compared between two groups using the Fisher exact test. The relations of continuous variables between or among groups were compared using a t test or one-way ANOVA, respectively. For multiple testing, Bonferroni correction was employed. The relations between tumor volume curves were compared using two-way ANOVA. p values < 0.05 were considered statistically significant. All of the statistical details can be found in the figure legends.